Production of bottomonia states in proton-proton and heavy ion collisions

Vineet Kumar[d,*], Prashant Shukla[d,e], Abhijit Bhattacharyya[f]

aNuclear Physics Division, Bhabha Atomic Research Centre, Mumbai 400085, India
bHomi Bhabha National Institute, Anushakti Nagar, Mumbai 400094, India
cDepartment of Physics, University of Calcutta, 92, A. P. C. Road Kolkata-700009, India

Abstract

This work reviews bottomonia production process in high energy hadronic collisions to investigate the fundamental aspects of Quantum Chromodynamics. Emphasis is given to the lessons learnt from the LHC data, which are reviewed in a global prospective with the results from the RHIC at lower energies used for comparison. The review covers bottomonia production in proton-proton, proton-nucleus and nucleus-nucleus collisions and includes discussion of the effects of hot and cold strongly interacting matter.

Keywords: Beauty, Quarkonium, Bottomonium, Hadron Collision, Heavy-Ion Collision, Quark-Gluon Plasma, LHC, RHIC

Contents

*Corresponding author

Email address: vineetk@barc.gov.in (Vineet Kumar)

Production of bottomonia states in proton-proton and heavy ion collisions

Vineet Kumar[d,*], Prashant Shukla[d,e], Abhijit Bhattacharyya[f]

[d]*Nuclear Physics Division, Bhabha Atomic Research Centre, Mumbai 400085, India*
[e]*Homi Bhabha National Institute, Anushakti Nagar, Mumbai 400094, India*
[f]*Department of Physics, University of Calcutta, 92, A. P. C. Road Kolkata-700009, India*

1. Introduction

The strong interaction amoung quarks and gluons is described by Quantum Chromodynamics (QCD) that has two aspects; asymptotic freedom at short distance and colour confinement at long distances. At short distance perturbative methods are well applied but confinement is a non-perturbative phenomenon which is not very well understood yet. The study of quarkonia ($Q\bar{Q}$) serves as an effective tool to look at both of these perturbative and non-perturbative aspects of QCD.

It is expected that strongly interacting matter shows qualitatively new behavior at temperatures and/or densities which are comparable to or larger than the typical hadronic scale. It has been argued that under such extreme conditions deconfinement of quarks and gluons should set in and the thermodynamics of strongly-interacting matter could then be understood in terms of these elementary degrees of freedom. This new form of matter is called quark-gluon plasma [1, 2], or QGP. The existence of such a transition has indeed been demonstrated from first principles using simulations of lattice QCD. The deconfinement transition and the properties of hot, strongly-interacting matter can be studied experimentally in heavy-ion collisions [3]. A significant part of the extensive experimental heavy-ion program is dedicated to measuring quarkonium yields since Matsui and Satz suggested that quarkonium suppression could be a signature of deconfinement [4]. In fact, the observation of anomalous suppression was considered to be a key signature of deconfinement at SPS energies [5].

One of the great opportunities of the LHC heavy-ion program is the ability to study bottomonium yields. From a theoretical perspective, bottomonium is an important and clean probe for at least two reasons. First, the effective field theory approach, which provides a link to first principles QCD, is more applicable for bottomonium due to better separation of scales and higher dissociation temperatures. Second, the heavier bottom quark mass reduces the importance of statistical recombination effects. Experimentally it has less

---

*Corresponding author
Email address: vineetk@barc.gov.in (Vineet Kumar)

background contribution and is easy to reconstruct. All these properties make bottomonium a good probe of QGP formation in heavy ion collisions.

There have been immense experimental [6, 7, 8, 9, 10] and theoretical works [11, 12, 13, 14] on quarkonia modifications in PbPb collisions. One of the most prominent signatures of QGP formation is that the production of quarkonia, the bound states of a heavy quark and its antiquark, is suppressed with respect to expectations from scaling the yields in proton-proton collisions by the number of binary nucleon-nucleon (NN) collisions. The extent of the quarkonia suppression is expected to be sequentially ordered by the binding energies of the quarkonia states. Because of the binding energy dependence of the screening, the bottomonium states (Υ(1S), Υ(2S), Υ(3S), χ_b, etc.) are particularly useful probes to understand the color screening properties of the QGP. The sequential suppression of the yield of Υ(nS) states was first observed by CMS at $\sqrt{s_{NN}}$ =2.76 TeV [15, 16]. More recently, results with improved statistical precision have been reported by both the ALICE [17] and CMS Collaborations [7, 8] at $\sqrt{s_{NN}}$ =5.02. The suppression of the Υ(1S) meson has also been studied at $\sqrt{s_{NN}}$ =200 GeV at RHIC [18] although the bottomonia production cross section is small at lower energies.

In this writeup we review experimental and theoretical aspects of bottomomia production in pp, pA and AA collisions at RHIC and LHC energies.

2. Bottomonia production p-p collisions: Experimental overview

Here all description of measured data of bottomonium should come. Take from NRQCD paper

I put data from Tevatraon and LHC. The language need to be reconciled at the end. (Vineet)

Heavy-flavour production in pp collisions provides important tests of our understanding of various aspects of QCD. The heavy-quark mass acts as a long distance cut-off so that the partonic hard-scattering process can be calculated in the framework of perturbative QCD down to low transverse momenta. When the heavy-quark pair forms a quarkonium bound state, this process is non-perturbative as it involves long distances and soft momentum scales. Therefore, the detailed study of heavy-flavour production and the comparison to experimental data provides an important testing ground for both perturbative and non-perturbative aspects of QCD calculations.

The Υ meson was discovered by E288 collaboration at Fermilab in 400 GeV proton nucleus collisions in 1977 [19]. The Collider Detector at Fermilab (CDF) reports Υ(1S), Υ(2S) and Υ(3S) differential ($d^2\sigma/dp_T dy$) and integrated cross sections in p$\overline{\text{p}}$ collisions at $\sqrt{s}$ = 1.8 TeV [20]. The three resonances were reconstructed through the decay of Υ(nS) to μ^+ and μ^-. The differential ($d^2\sigma/dp_T dy$) and integrated

Table 1: CDF Run I Υ cross section measurement with luminosity of 16.6 pb^{-1} with $|y|<0.4$ at $\sqrt{s}$ = 1.8 TeV.

Υ(nS) state	$\frac{d\sigma(\Upsilon(nS))}{dy} \times B(\Upsilon(nS) \to \mu^+\mu^-)$ (pb)
Υ(1S)	753±29(stat.)±72(syst.)
Υ(2S)	183±18(stat.)±24(syst.)
Υ(3S)	101±15(stat.)±13(syst.)

Table 2: CDF Run I Υ cross section measurement with luminosity of 77.0 pb^{-1} with $|y|<0.4$ at $\sqrt{s}$ = 1.8 TeV.

Υ(nS) state	$\frac{d\sigma(\Upsilon(nS))}{dy} \times B(\Upsilon(nS) \to \mu^+\mu^-)$ (pb)
Υ(1S)	680±15(stat.)±18(syst.)±26(lumi.)
Υ(2S)	175±9(stat.)±8(syst.)
Υ(3S)	97±8(stat.)±5(syst.)

cross sections have measured in the range 0<p_T<16 GeV/c for Υ(1S) and in the range 0<p_T<10 GeV/c for Υ(2S) and Υ(3S). Table 1 summarizes the 1995 CDF Run I cross section measurement [20].

In 2002, CDF Run I measured both the Υ cross section and polarization with an integrated luminosity of 77 pb^{-1} [21]. The cross section results from the CDF Run I measurement from 2002 are listed in Table 2.

For Run II at the Tevatron at $\sqrt{s}$ = 1.96 TeV, only D0 has published a result. D0 Run II made an Υ cross section measurement in 2005 with a varying rapidity range and a luminosity of 185 pb^{-1} [22]. Table 3 summarizes the D0 Run II Υ cross section measurement

The next set of measurements were done at the Large Hadron Collider (LHC) at $\sqrt{s}$ = 7 TeV in pp collisions. CMS measured the Υ cross section in 2011 with a luminosity of 3.1 pb^{-1}, rapidity range $|y|<$ 2, and $p_T<$ 30 GeV [23]. Table 4 shows the CMS measurement of Υ cross-section.

In 2013, CMS again measured the Υ cross section but with a luminosity of 35.8 pb^{-1}, rapidity of $|y|<$ 2.4 and $p_T<$ 50 GeV [24] as shown in Table 5.

Table 3: D0 Run II Υ(1S) cross section measurement with luminosity of 185.0 pb^{-1} with different rapidity ranges at $\sqrt{s}$ = 1.96 TeV [22].

rapidity range	$\frac{d\sigma(\Upsilon(1S))}{dy} \times B(\Upsilon(nS) \to \mu^+\mu^-)$ (pb)
0.0-0.6	628±16(stat.)±63(syst.)±38(lumi.)
0.6-1.2	654±17(stat.)±65(syst.)±40(lumi.)
1.2-1.8	515±16(stat.)±46(syst.)±31(lumi.)
0.0-1.8	597±12(stat.)±58(syst.)±36(lumi.)

Table 4: CMS measurement of Υ(nS) cross section with luminosity of 3.1 pb^{-1} in $|y|<$ 2.0 and p$_T<$ 30 GeV at $\sqrt{s}$=7 TeV [23].

Υ(nS) state	$\sigma(pp \rightarrow \Upsilon(nS)X) \times B(\Upsilon(nS) \rightarrow \mu^+\mu^-)$ (nb)
Υ(1S)	7.37 ± 0.13(stat.)$^{+0.61}_{-0.42}$(syst.)±0.81(lumi.)
Υ(2S)	1.90 ± 0.09(stat.)$^{+0.20}_{-0.14}$(syst.)±0.24(lumi.)
Υ(3S)	1.02 ± 0.07(stat.)$^{+0.11}_{-0.08}$(syst.)±0.11(lumi.)

Table 5: CMS measurement of Υ(nS) cross section in $|y|<$ 2.4 and p$_T<$ 50 GeV at $\sqrt{s}$=7 TeV [24].

Υ(nS) state	$\sigma(pp \rightarrow \Upsilon(nS)X) \times B(\Upsilon(nS) \rightarrow \mu^+\mu^-)$ (nb)
Υ(1S)	8.55 ± 0.05(stat.)$^{+0.56}_{-0.50}$(syst.)±0.34(lumi.)
Υ(2S)	2.21 ± 0.03(stat.)$^{+0.16}_{-0.14}$(syst.)±0.09(lumi.)
Υ(3S)	1.11 ± 0.02(stat.)$^{+0.10}_{-0.08}$(syst.)±0.04(lumi.)

The ATLAS measured the Υ(nS) production cross section with a luminosity of 1.8 fb^{-1}, rapidity of $|y|<$ 2.25, and p$_T<$ 70 GeV [25]. The results are shown in table 6.

Several Υ polarization measurements have now also been made. With a luminosity of 77 pb^{-1}, CDF Run I measured the Υ(1S) polarization in 2002 at $\sqrt{s}$ = 1.8 TeV with $|y|<$ 0.4 and found the Υ(1S) to be unpolarized [21]. At $\sqrt{s}$ = 1.96 TeV, D0 Run II measured the Υ(1S) and Υ(2S) polarization in 2008 in a sample with luminosity of 1.3 fb^{-1} [26]. The measurement done by D0 found longitudinal polarization for the Υ(1S) [26]. However, these first polarizations measurements were only measured in one reference frame, and the results could be biased due to the choice of the reference frame and the acceptance of the detector. Newer measurements were done in multiple reference frames and include the calculation of the frame invariant parameter to prevent bias from detector acceptance with the choice of a single reference frame.

The first full polarization for all Υ(nS) states was measured in 2012 by CDF Run II at $\sqrt{s}$ = 1.96 TeV [27]. The CDF Run II measurement had a luminosity of 6.7 fb^{-1} with $|y|<$ 0.6 and p$_T<$ 40 GeV

Table 6: ATLAS measurement of Υ(nS) cross section in $|y|<$ 2.25 and p$_T<$ 70 GeV at $\sqrt{s}$=7 TeV [25].

Υ(nS) state	$\sigma(pp \rightarrow \Upsilon(nS)X) \times B(\Upsilon(nS) \rightarrow \mu^+\mu^-)$ (nb)
Υ(1S)	8.01 ± 0.02(stat.)±0.36(syst.)±0.31(lumi.)
Υ(2S)	2.05 ± 0.01(stat.)±0.12(syst.)±0.08(lumi.)
Υ(3S)	0.92 ± 0.01(stat.)±0.07(syst.)±0.04(lumi.)

and also found no evidence for polarization [27]. CMS measured the Υ(nS) polarization in 2013 using a luminosity of 4.9 fb^{-1} at $\sqrt{s}$ = 7 TeV [28]. The CMS polarization measurement found the Υ to be unpolarized, and suggested that this could be a result of including Υ produced in feeddown from an excited state [28]. Improved Υ polarization measurements with lower uncertainties will allow theories to develop to provide insight into the quarkonium production mechanism.

The study of bottomonium production at LHC energies offers many advantages. First, there is no beauty feed-down. Second, owing to their larger masses, their decay products - usually leptons - are more energetic and more easily detectable (detector acceptance, trigger bandwidth, etc.). Third, the existence of three sets of bottomonia with their principal quantum number n = 1, 2, 3 below the open-beauty threshold offers a wider variety of states that can be detected in the dilepton decay channel this, however, introduces a complicated feed-down pattern.

With the advent of the LHC, the study of Υ production has become more accessible than ever. The Υ production pattern at the LHC differs from that of the lighter ψ's. The Υ's having three states with different binding energies are thus far richer probes of the QCD dynamics in pp and PbPb collisions than the charmonia. It is therefore important to achieve a good understanding of their production mechanism in the vacuum as well as of how the nuclear effects in proton-nucleus collisions affect them. In this section we will give an overview of measurements of Υ production in pp collisions at LHC.

The measurements of Υ(1S,2S,3S) production in pp collisions at the unprecedented C.M. energies of 2.76, 5.02, 7, 8, and 13 TeV have been undertaken, within the rapidity window -2.4< y < 4.5 and the dimuon momentum range of p$_T$ < 100 GeV/c at LHC by ALICE [29, 25], ATLAS [29, 25], CMS [30, 31] and LHCb collaborations.

In addition, the angular distribution of the muons produced in the Υ(1S, 2S, 3S) decays has been analyzed in different reference frames to determine the polarization parameters. From the results of CMS and LHCb, Υ(1S, 2S, 3S) polarization parameters are all so close to zero that polarizations can be neglected. The measurements of these cross sections and polarizations have shed light on the Υ(1S, 2S, 3S) production mechanisms in pp collisions. Analysis of new LHC data will extend the reach of the kinematics to test the NRQCD with higher-order corrections which becomes more sensitive with the increase of p$_T$,

3. Bottomonia production mechanism in p-p collisions

In general one can subdivide the quarkonia production process into two major parts

1. Production of a heavy quark pair in hard collisions.

2. Formation of quarkonia out of the two heavy quarks.

The massive quarks (with $m_c \sim 1.6$ GeV/c^2, $m_b \sim 4.5$ GeV/c^2) are produced in initial stages in hadronic collision with high momentum transfer and thus can be treated perturbatively [32]. The emergence of quarkonia out of the two massive quarks, on the other hand can only be described non-perturbatively using different models [33, 34]. The Colour Singlet Model (CSM) [35, 36], Colour Evaporation Model (CEM) [37, 38], the Fragmentation Scheme and the NRQCD factorisation formalism are some of the well established models for quarkonia production.

Due to the high mass of the heavy quarks they are produced in the initial collisions as their production requires sufficiently high momentum transfers. For this reason the heavy quark production is a hard process that can be treated perturbatively. The hadronic cross section in pp collisions can be written as

$$\sigma_{pp}(s, m^2) = \sum_{i,j=q,\bar{q},g} \int dx_1 \, dx_2 \, f_i^p(x_1, \mu_F^2) \, f_j^p(x_2, \mu_F^2) \, \widehat{\sigma}_{ij}(s, m^2, \mu_F^2, \mu_R^2) \tag{1}$$

where x_1 and x_2 are the fractional momenta carried by the colliding partons and f_i^p are the proton parton densities. The total partonic cross section has been completely calculated up to NLO [39, 32]. The partonic cross section is given by

$$\begin{aligned}
\widehat{\sigma}_{ij}(s, m, \mu_F^2, \mu_R^2) = & \; \frac{\alpha_s^2(\mu_R^2)}{m^2} \left\{ f_{ij}^{(0,0)}(\rho) \right. \\
& + \left. 4\pi\alpha_s(\mu_R^2) \left[f_{ij}^{(1,0)}(\rho) + f_{ij}^{(1,1)}(\rho) \ln\left(\frac{\mu_F^2}{m^2}\right) \right] + \mathcal{O}(\alpha_s^2) \right\}
\end{aligned} \tag{2}$$

where $\rho = 4m^2/s$ and $f_{ij}^{(k,l)}$ are the scaling functions to NLO [39, 32]. At small ρ, the $\mathcal{O}(\alpha_s^2)$ and $\mathcal{O}(\alpha_s^3)$ $q\bar{q}$ and the $\mathcal{O}(\alpha_s^2)$ gg scaling functions become small while the $\mathcal{O}(\alpha_s^3)$ gg and qg scaling functions plateau at finite values. Thus, at collider energies, the total cross sections are primarily dependent on the small x parton densities and phase space. The total cross section does not depend on any kinematic variables, only on the quark mass, m, and the renormalization and factorization scales with central value $\mu_{R,F} = \mu_0 = m$.

The nonperturbative evolution of the $Q\bar{Q}$ pair into a quarkonium has been discussed extensively in terms of models and in terms of the language of effective theories of QCD [33, 40]. Different treatments of this evolution have led to various theoretical models for inclusive quarkonium production. Most notable among these are the color-singlet model (CSM), the color-evaporation model (CEM) and the non-relativistic QCD (NRQCD) factorization approach. In this review we will mainly discuss the NRQCD approach, as theoretically, it is the most modern and acceptable one. However, we will touch upon CSM and CEM briefly.

3.1. The color singlet model

The color singlet model (CSM) was first proposed shortly after the discovery of the J/ψ [35, 41, 42, 36]. In this model, it is assumed that the $Q\bar{Q}$ pair that evolves into the quarkonium is in a color-singlet state and that it has the same spin and angular-momentum quantum numbers as the quarkonium. In the CSM, the production rate for each quarkonium state is related to the absolute values of the color-singlet $Q\bar{Q}$ wave function and its derivatives, evaluated at zero $Q\bar{Q}$ separation. These quantities can be extracted by comparing theoretical expressions for quarkonium decay rates in the CSM with experimental measurements. Once this extraction has been carried out, the CSM has no free parameters. The CSM was successful in predicting quarkonium production rates at relatively low energy [43]. Recently, it has been found that, at high energies, very large corrections to the CSM appear at next-to-leading order (NLO) and next-to-next-to-leading order (NNLO) in α_s [44, 45, 46]. Consequently, the possibility that the CSM might embody an important production mechanism at high energies has re-emerged. However, given the very large corrections at NLO and NNLO, it is not clear that the perturbative expansion in α_s is convergent.

3.2. The color evaporation model

The CEM [37, 38, 47] is motivated by the principle of quark-hadron duality. In the CEM, it is assumed that every produced $Q\overline{Q}$ pair evolves into a quarkonium if it has an invariant mass that is less than the threshold for producing a pair of open-flavor heavy mesons. It is further assumed that the nonperturbative probability for the $Q\overline{Q}$ pair to evolve into a quarkonium state H is given by a constant F_H that is energy-momentum and process independent. Once F_H has been fixed by comparison with the measured total cross section for the production of the quarkonium H, the CEM can predict, with no additional free parameters, the momentum distribution of the quarkonium production rate. The CEM predictions provide good descriptions of the CDF data for J/ψ, $\psi(2S)$, and χ_c production at $\sqrt{s} = 1.8$ TeV [47].

The heavy quark production cross section are calculated to NLO in pQCD using the CT10 parton densities [48]. The mass and scale parameters used for open and hidden heavy flavor production are obtained by fitting the energy dependence of open heavy flavor production to the measured total cross sections [49]. The botttom quark mass and scale parameters are $m_b = 4.65 \pm 0.09$ GeV, $\mu_F/m_{Tb} = 1.40^{+0.75}_{-0.47}$, and $\mu_R/m_{Tb} = 1.10^{+0.26}_{-0.19}$. The quarkonium production cross sections are calculated in the color evaporation model with normalizations determined from fitting the scale parameter to the shape of the energy-dependent cross sections [49]. The central EPS09 NLO parameter set [50] is used to calculate the modifications of the parton distribution functions (nPDF) in Pb+Pb collisions, referred as cold nuclear

9

Table 7: Heavy quark and quarkonia production cross sections at $\sqrt{s_{NN}} = 5.02$ TeV. The cross sections are given per nucleon pair while N^{PbPb} gives the initial number of heavy quark pair/quarkonia per Pb+Pb event.

	$b\bar{b}$	Υ
σ_{pp}	$210.3^{+70.8}_{-77.6}$ μb	$0.42^{+0.14}_{-0.16}$ μb
σ_{PbPb}	$179.3^{+60.3}_{-66.2}$ μb	$0.359^{+0.121}_{-0.132}$ μb
N^{PbPb}	$1.007^{+0.339}_{-0.372}$	$0.0020^{+0.0007}_{-0.0007}$

matter (CNM) effects. The production cross sections for heavy flavor and quarkonia at $\sqrt{s_{NN}} = 2.76$ TeV [51] are given in Table 7. The yields in a minimum bias Pb+Pb event is obtained from the per nucleon cross section, σ_{PbPb}, in Table 7, as

$$N = \frac{A^2 \sigma_{\mathrm{PbPb}}}{\sigma^{\mathrm{tot}}_{\mathrm{PbPb}}} \ . \tag{3}$$

At 2.76 TeV, the total Pb+Pb cross section, $\sigma^{\mathrm{tot}}_{\mathrm{PbPb}}$, is 7.65 b [52].

3.3. The NRQCD factorization approach

In the framework of CSM, the $Q\bar{Q}$ pair, eventually evolving into the quarkonium, is assumed to be in Colour Singlet (CS) state and that has spin and angular momentum same as that of quarkonium. Apart from comprising of the CSM, the NRQCD factorisation approach incorporates the Colour Octet (CO) states as well.

In the formalism of the NRQCD factorisation approach, the evolution probability of $Q\bar{Q}$ pair into a state of quarkonium is expressed as matrix elements of NRQCD operators expanded in terms of heavy quark velocity v (for $v \ll 1$) [33]. The factorisation formulae were then used to calculate production cross-sections and decay rates of quarkonia states. The full structure of the $Q\bar{Q}$ Fock space is considered and spanned by $n = {}^{2s+1}L_J^{[a]}$ state where s is the spin, L is the orbital angular momentum, J is the total angular momentum and a (colour multiplicity) = 1 for CS and 8 for CO states. The produced CO states of $Q\bar{Q}$ pair at short distances emerge as CS quarkonia by emitting soft gluons non-perturbatively.

There have been several works on bottomonia production based on NRQCD formalism [53, 54, 55, 56, 57]. Both production and polarisation of Υ(nS) at NLO have been discussed in Ref. [58] within the framework of NRQCD. The CO matrix elements are obtained by fitting with experimental data. The study is updated in Ref. [59] by considering feed down from χ_{bJ}(mP) states in Υ(nS) production. The yields and polarisations of Υ(nS) measured at Tevatron and LHC are well explained by this work. The NLO study in Ref. [60] describes the yields and polarisations of Υ(nS) at LHC which includes feed down contributions

from higher states. In Ref. [61], production cross-section for Υ(nS), χ_{bJ}, η_b and h_b have been calculated using NRQCD, as produced in hard photo production and fragmentation processes at LHC energies.

A LO NRQCD analyis is useful as it is straightforward and unique and once the parameters are obtained by fitting over large datasets it has excellent predictability power for unknown cross sections. It is shown that there is a large difference amoung the LDMEs obtained by different analysis at NLO. The LO NRQCD calculations for the differential production cross-sections of Υ states in p+p collisions also have been presented. A large set of data from Tevatron [62] and LHC [63, 64, 65, 66, 67] is used to extract the LDMEs required for the Υ production.

The processes that govern the differential production of heavy mesons like bottomonium, as functions of p_T are mostly 2→2 operations. These processes can be denoted generically by $i + j \rightarrow \Upsilon + X$, where i and j are the incident light partons, Υ is the heavy meson and X is final state light parton. The double differential cross-section as a function of p_T and rapidity (y) of the heavy meson can be written as [68],

$$E \frac{d^3\sigma^\Upsilon}{d^3p} = \sum_{i,j} \int dx_1 dx_2 f_{i/p}(x_1, \mu_F^2) f_{i/p}(x_2, \mu_F^2) \delta(s+u+t-m^2) \frac{\hat{s}}{\pi} \frac{d\sigma}{d\hat{t}}$$

where, $f_{i/p}(f_{j/p})$ are the colliding parton $(i(j))$ distribution functions in the incident protons. They depend on the fractions $x_1(x_2)$, of the total momentum carried by the incident partons and the scale of factorisation μ_F. Here $\sqrt{s}$ represents the total center of mass energy of the pp system and m_T $(= \mu_F)$ stands for the transverse mass, $m_T^2 = p_T^2 + M^2$ of the quarkonium. The $d\sigma/d\hat{t}$ in Eq. 4 is the parton level cross-section and is defined as [33],

$$\frac{d\sigma}{d\hat{t}} = \frac{d\sigma}{d\hat{t}}(ab \rightarrow Q\bar{Q}(^{2s+1}L_J) + X) M_L(Q\bar{Q}(^{2s+1}L_J) \rightarrow \Upsilon) \tag{4}$$

The first term in RHS is the short distance contribution, that corresponds to the $Q\bar{Q}$ pair production in specific colour and spin configuration and is calculable using perturbative QCD (pQCD) [55, 69, 70, 71, 72, 73]. The other term in the RHS of Eq.(4) is the Long Distance Matrix Element (LDME) and refers to the probability of the $Q\bar{Q}$ state to convert into a quarkonium state. They are determined by contrasting with experimental observations.

The NRQCD formalism provides an adequate procedure to estimate a quantity as an expansion in heavy quark relative velocity, v inside $Q\bar{Q}$ bound state. The LDME in Eq.(4) do scale with definitive power in v. The quarkonium yield depends on the $^3S_1^{[1]}$ and $^3P_J^{[1]}$(J=0,1,2) CS states and $^1S_0^{[8]}$, $^3S_1^{[8]}$ and $^3P_J^{[8]}$ CO states in the limit $v \ll 1$. The superscripts in square brackets represent the colour structure of the bound state, 1 for the CS and 8 for the CO.
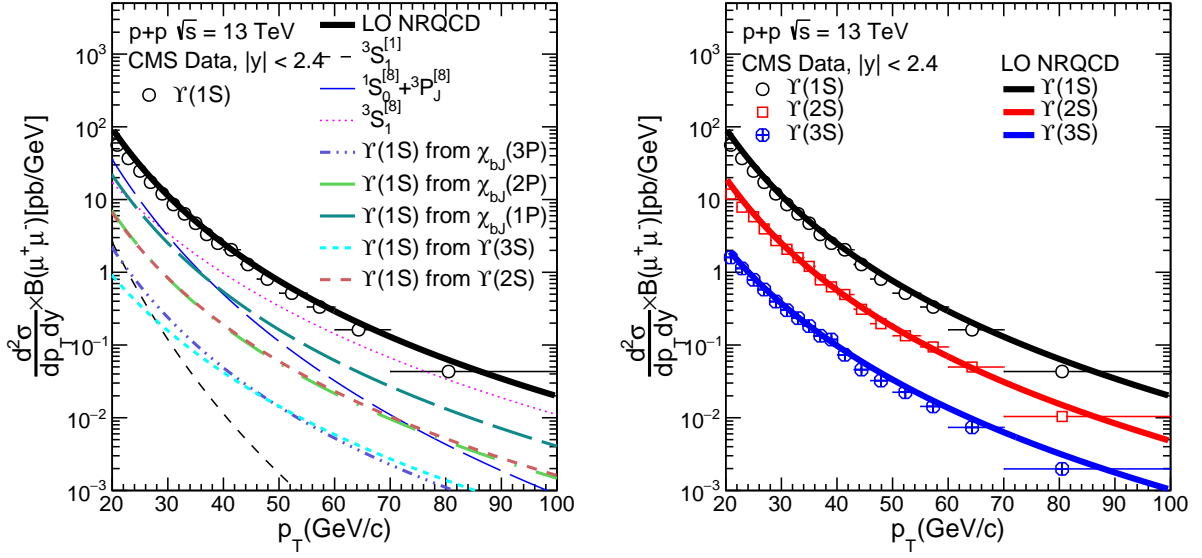
Figure 1: The NRQCD calculations of production cross-section of Υ(nS) in p+p collisions at $\sqrt{s}$ = 13 TeV in central rapidities, as a function of transverse momentum compared with the measured data at CMS [67] experiment. The left figure shows relative contributions in Υ(1S) from singlet and octet states as well as from feeddown. The right figure shows the sum of all contributions for all the 3 states where the results for Υ(1S) and Υ(2S) are shifted vertically by a constant factor for better visibility.
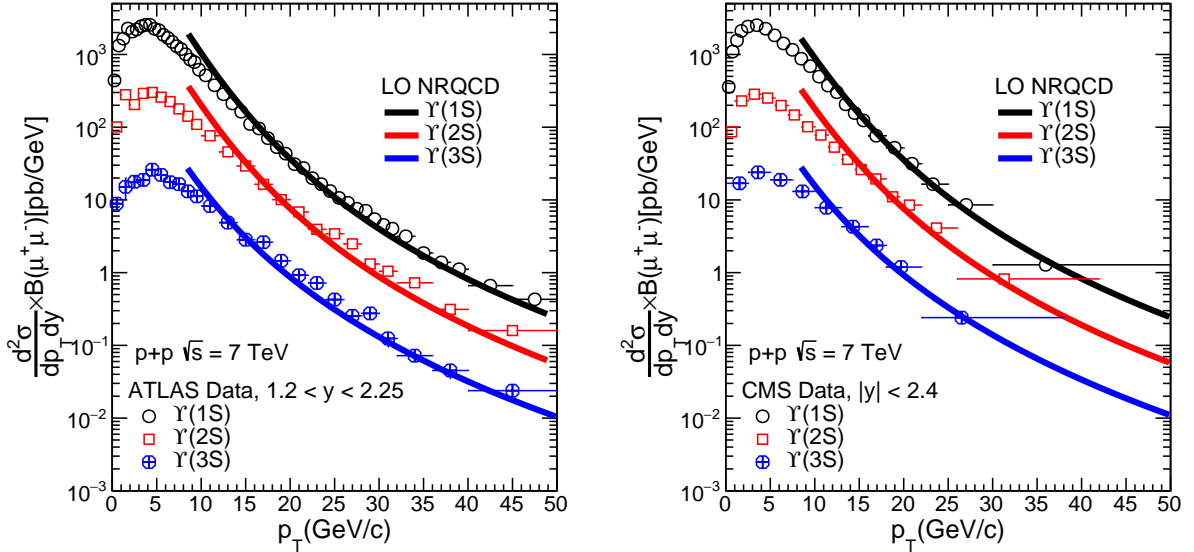

Figure 2: The NRQCD calculations of production cross-section of Υ(nS) in p+p collisions at $\sqrt{s}$ = 7 TeV, as a function of transverse momentum compared with the measured data by ATLAS [65] in left figure and CMS [66] in right figure. The cross-section of Υ(1S) and Υ(2S) as well as calculations are shifted vertically by a constant factor for better visibility.

Table 8: Comparison of CS elements and CO LDMEs extracted from fitting with experimental data using NRQCD formalism for $\Upsilon(1S)$.

Ref. (LO/NLO)	PDF	m_b (GeV)	$M_L(b\bar{b}([^3S_1]_1 \to \Upsilon(1S))$ (GeV^3)	$M_L(b\bar{b}([^3S_1]_8 \to \Upsilon(1S))$ (GeV^3)	$M_L(b\bar{b}([^1S_0]_8, [^3P_0]_8 \to \Upsilon(1S))$ (GeV^3)	p_T-cut GeV/c
present (LO)	CT18	4.88	10.9	0.0601±0.0017	0.0647±0.0016	8
[54] (LO)	CTEQ4L	4.88	11.1	0.077±0.017	0	2
				0.087±0.016	0	4
				0.106±0.013	0	8
[55] (LO)	CTEQ5L	4.77	12.8±1.6	0.116±0.027	0.109±0.062	8
				0.124±0.025	0.111±0.065	
	MRSTLO	4.77	12.8±1.6	0.117±0.030	0.181±0.072	8
				0.130±0.028	0.186±0.075	
[57] (LO)	MSTW08LO	4.88	10.9	0.0477±0.0334	0.0121±0.0400	-
[58] (NLO)	CTEQ6M	4.75	9.282	-0.0041±0.0024	0.0780±0.0043	8
[59] (NLO)	CTEQ6M	PDG	9.282	0.0061±0.0024	0.0895±0.0248	8

We require both CS and CO matrix elements in order to get theoretical predictions for the production of bottomonia at the Tevatron and LHC energies. The corresponding expressions and numerical values for CS states are obtained from Ref. [55]. The CO states, on the other hand, cannot be directly connected to the non-relativistic wavefunctions of heavy mesons, as these are associated with a higher Fock state. Experimentally measured data sets are therefore employed to obtain them as in Refs. [55, 72, 73]. For the CO elements related to p-wave states, needed as the feed down contributions, we have used values obtained by Ref. [57, 59] for the present purpose. In our calculations, we have used CT18NLO parametrisation [74] for parton distribution functions and the bottom quark mass m_b is taken to be 4.88 GeV.

Figure 1 shows the NRQCD calculations of production cross-section of Υ(nS) in p+p collisions at $\sqrt{s}$ = 13 TeV in central rapidities, as a function of transverse momentum compared with the measured data at CMS [67] experiment. The left figure shows relative contributions in Υ(1S) from singlet and octet states as well as from feeddown. The right figure shows the sum of all contributions for all the 3 states where the results for Υ(1S) and Υ(2S) are shifted vertically by a constant factor for better visibility.

Figure 2 shows the NRQCD calculations of production cross-section of Υ(nS) in p+p collisions at $\sqrt{s}$ = 7 TeV, as a function of transverse momentum compared with the measured data by ATLAS [65] in left figure and CMS [66] in right figure. The cross-section of Υ(1S) and Υ(2S) as well as calculations are shifted vertically by a constant factor

for better visibility.

Table 8 shows our results for Υ(1S) parameters along with the results from different groups. The individual values of LDMEs are in agreement with the values from previous works but with considerable reduction in errors upon inclusion of 13 TeV data sets from CMS.

We have presented NRQCD calculations for the differential production cross-sections of Υ states in p+p collisions. Measured transverse momentum distributions of Υ(3S), Υ(2S) and Υ(1S) in p $+\bar{\text{p}}$ collisions at $\sqrt{s} = 1.8$ TeV and in p+p collisions at 7 TeV and 13 TeV are used to constrain the LDMEs. All the relevant feeddown contributions from higher mass states including the χ_b(3P) are taken in to account. The calculations for Υ(3S), Υ(2S) and Υ(1S) are compared with the measured data at Tevatron and LHC. The formalism provides very good description of the data in large transverse momentum range at different collision energy. We compare the LDMEs for bottomonia obtained in this analysis with the results from earlier works. At high p_T, the colour singlet contribution is very small and LHC data in large p_T range help to constrain the relative contributions of different colour octet contributions.

These values will be useful for predictions of quarkonia cross-section and for the purpose of a comparison with those obtained using the NLO formulations.

4. Experimental overview of Bottomonia results at RHIC and LHC

4.1. Υ(nS) R_{AA}

The available experimental data, spanning from 0.20 to 5.02 TeV, have provided new insight into the thermal properties of the QGP. In this section we review the current status of the experimental measurement of R_{AA} and v_2 for Υ states. The data from different experiments are comapred and physics insights from them is discussed.

Measurement by CMS, ATLAS and ALICE. The bottomonia states (Υ(nS)) are measured at the LHC with very good statistical precision [16, 75, 15, 76]. The CMS measurements at $\sqrt{s_{NN}}$ =2.76 TeV [16, 15] reveal a clear proof of sequential suppression : Υ(2S) and Υ(3S) are more suppressed relative to the ground state Υ(1S). The individual Υ states are also found to be suppressed in the PbPb collisions relative to the production in the pp collisions. The Υ nuclear modification factor, R_{AA}, shows a strong dependence on collision centrality but has weak dependence on Υ meson p_T and rapidity [76]. The forward rapidity ($2.5 \leq y^{\Upsilon} \leq 4.0$) measurement of the Υ suppression at ALICE [75] is found to be consistent with the midrapidity ($|y^{\Upsilon}| \leq 2.4$) measurement of the Υ suppression at the CMS. The CMS and ALICE collaborations have carried out the R_{AA} measurement of Υ at $\sqrt{s_{NN}} = 5.02$ TeV with the Run II LHC PbPb collisions [8, 7, 17]. The CMS experiment measured slightly more amount of Υ suppression at $\sqrt{s_{NN}} = 5.02$ TeV [8, 7] than the suppression at $\sqrt{s_{NN}} = 2.76$ TeV [76] while the ALICE experiment observed less suppression at $\sqrt{s_{NN}} = 5.02$ TeV than that at $\sqrt{s_{NN}} = 2.76$ TeV in the most central PbPb collisions [75, 17].

Figure 3 shows the Υ(nS) nuclear modification factor, R_{AA}, (a) as a function of transverse momentum p_T and (b) as a function of rapidity measured by CMS [77], ALICE [78] and ATLAS experiments [78]. The vertical bars denote statistical uncertainties, and the rectangular boxes show the total systematic uncertainties.
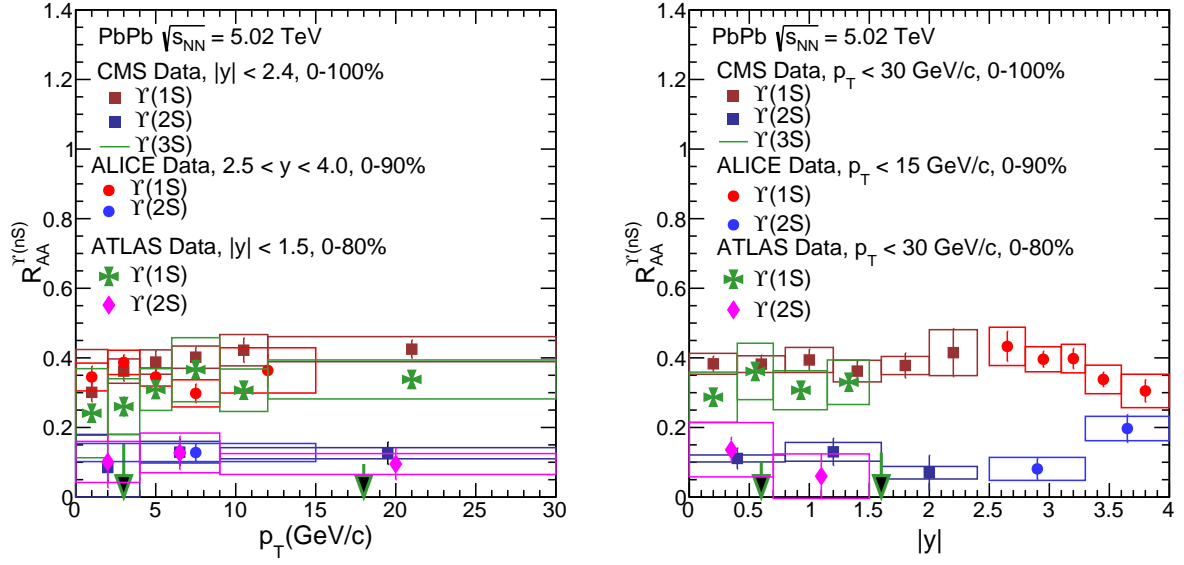
Figure 4 shows the Υ(nS) nuclear modification factor, R_{AA} as a function of N_{Part} measured by CMS [77], ALICE experiments [78] and ATLAS experiments [78]. The vertical bars denote statistical uncertainties and the rectangular boxes show the total systematic uncertainties.

Figure 3: (Color online) The Υ(nS) nuclear modification factor, R_{AA}, (a) as a function of transverse momentum p_T and (b) as a function of rapidity measured by CMS [77], ALICE [78] and ATLAS experiments [78]. The vertical bars denote statistical uncertainties, and the rectangular boxes show the total systematic uncertainties.
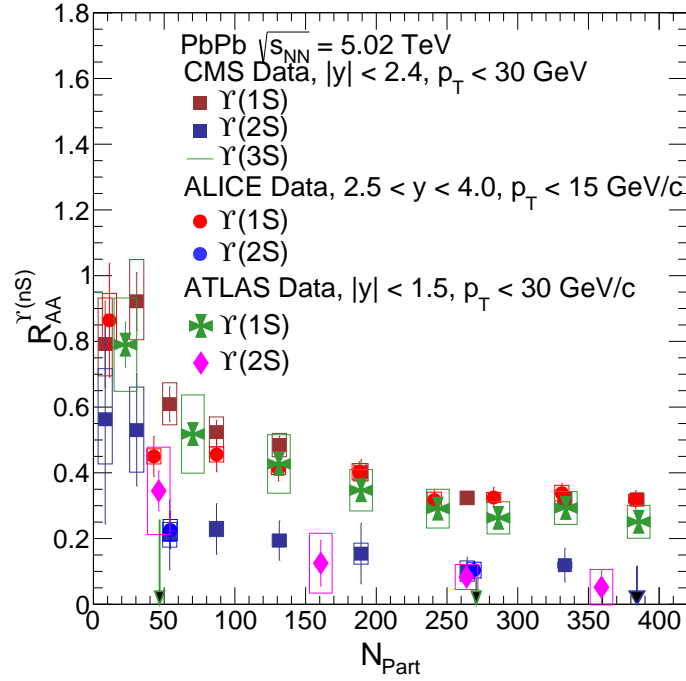

Figure 4: (Color online) The Υ(nS) nuclear modification factor, R_{AA} as a function of N_{Part} measured by CMS [77], ALICE experiments [78] and ATLAS experiments [78]. The vertical bars denote statistical uncertainties and the rectangular boxes show the total systematic uncertainties.
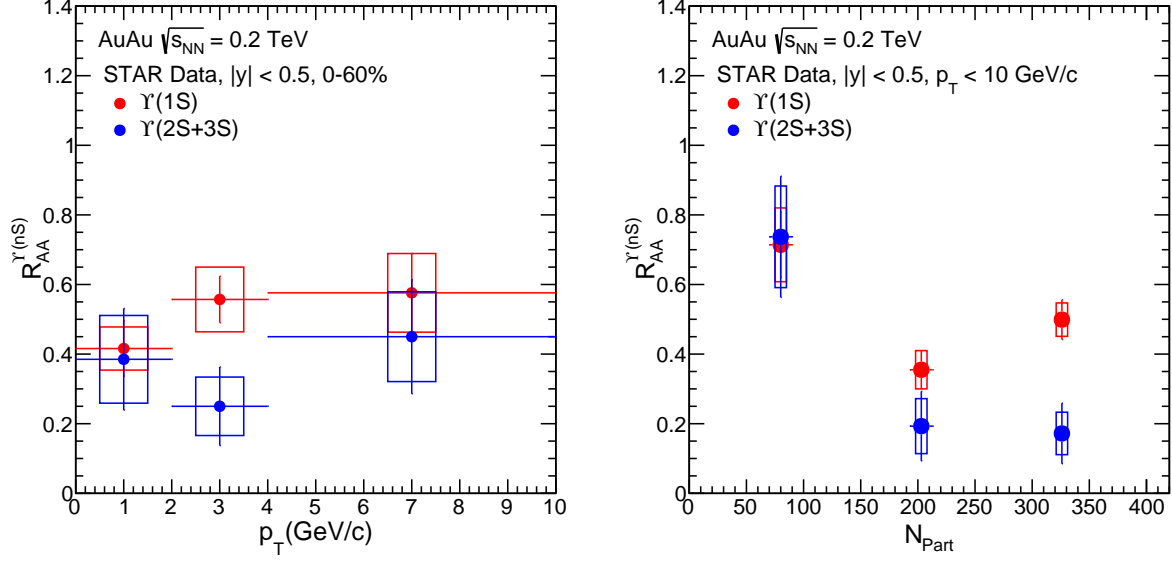
Figure 5: (Color online) The Υ(nS) nuclear modification factor, R_{AA}, (a) as a function of transverse momentum p_T and (b) as a function of N_{Part} measured by STAR experiments [79]. The vertical bars denote statistical uncertainties, and the rectangular boxes show the total systematic uncertainties.
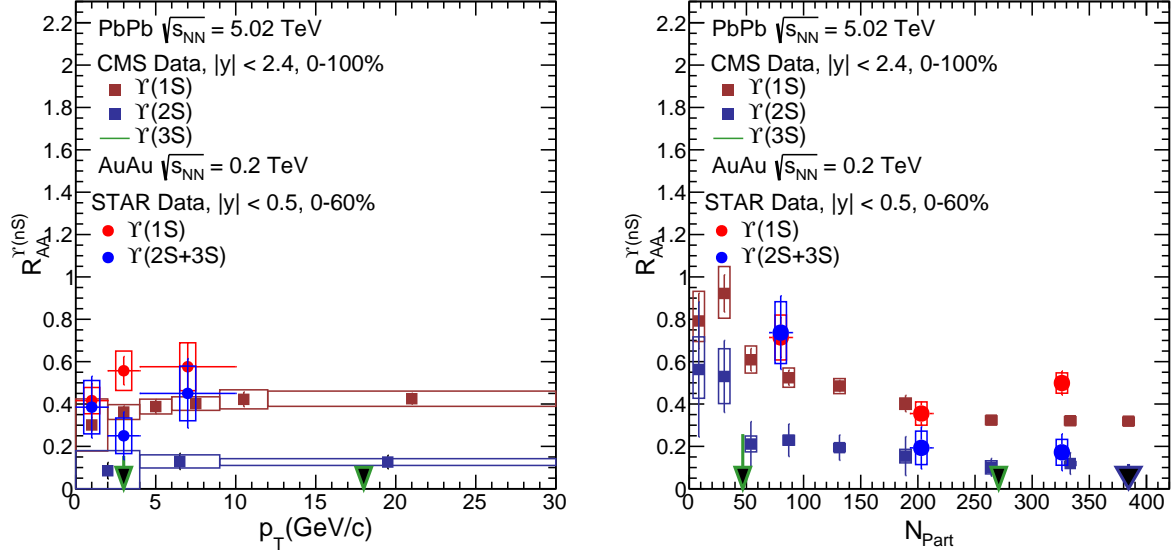

Figure 6: (Color online) The Υ(nS) nuclear modification factor, R_{AA}, (a) as a function of transverse momentum p_T and (b) as a function of N_{Part} measured by STAR experiments [79] at 0.2 TeV and CMS experiment [77] at 5.5 TeV. The vertical bars denote statistical uncertainties, and the rectangular boxes show the total systematic uncertainties.
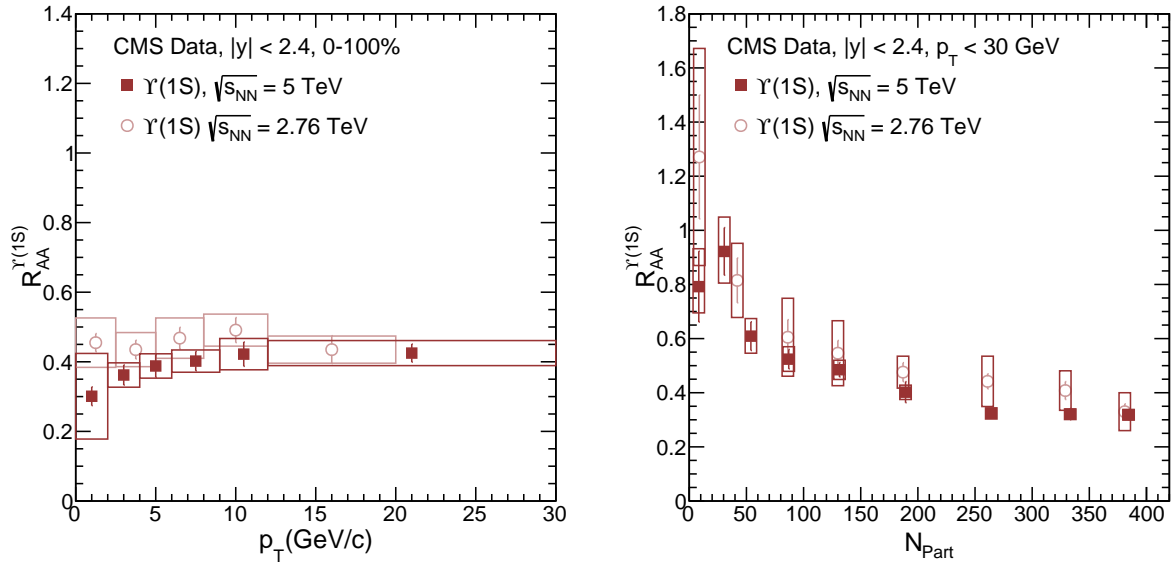
16

Figure 7: (Color online) The Υ(nS) nuclear modification factor, R_{AA}, (a) as a function of transverse momentum p_T and (b) as a function N_{Part} measured by CMS at 2.76 [76] and 5.02 TeV [77]

Figure 5 shows the Υ(nS) nuclear modification factor, R_{AA}, (a) as a function of transverse momentum p_T and (b) as a function of N_{Part} measured by STAR experiments [79]. The vertical bars denote statistical uncertainties, and the rectangular boxes show the total systematic uncertainties.

Figure 6 shows the Υ(nS) nuclear modification factor, R_{AA}, (a) as a function of transverse momentum p_T and (b) as a function of N_{Part} measured by STAR experiments [79] at 0.2 TeV and CMS experiment [77] at 5.5 TeV. The vertical bars denote statistical uncertainties, and the rectangular boxes show the total systematic uncertainties.

Figure 7 shows the Υ(nS) nuclear modification factor, R_{AA}, (a) as a function of transverse momentum p_T and (b) as a function N_{Part} measured by CMS at 2.76 [76] and 5.02 TeV [77]

4.2. Υ(nS) azimuthal anisotropy

The screening due to the QGP can also result in an azimuthal asymmetry in the observed yields of quarkonia. In non-central heavy ion collisions, the produced QGP has a lenticular shape in the transverse plane. Consequently, the average path length for quarkonia traveling through the medium depends on the direction taken with respect to this shape, with a larger suppression in the direction of the longer axis [80]. The anisotropic distribution of particles can be characterized by the magnitudes of the Fourier co-efficients (v_n) of the azimuthal correlation of particles [81]. By studying the azimuthal distribution of the quarkonia, it is possible to develop a more comprehensive understanding of the dynamics of their production.

The CMS experiment measured v_2 coefficients for Υ(1S) and Υ(2S) mesons in PbPb collisions at a nucleon-nucleon center-of-mass energy of 5.02TeV. Figure 8 shows the Υ(1S) azimuthal anisotropy (v_2) (a) as a function of collision centrality and (b) as a function of transverse momentum p_T measured by CMS experiment at LHC [82]. The p_T integrated results shown in Fig. 8 (a) for three centrality intervals are consistent with zero within the statistical uncertainties. The average v_2 values in the 10-90% centrality interval measured by CMS experiment are found to be 0.007±0.011(stat)±0.005(syst) for Υ(1S) and -0.063±0.085(stat)±0.037(syst) for Υ(2S). The p_T dependence of
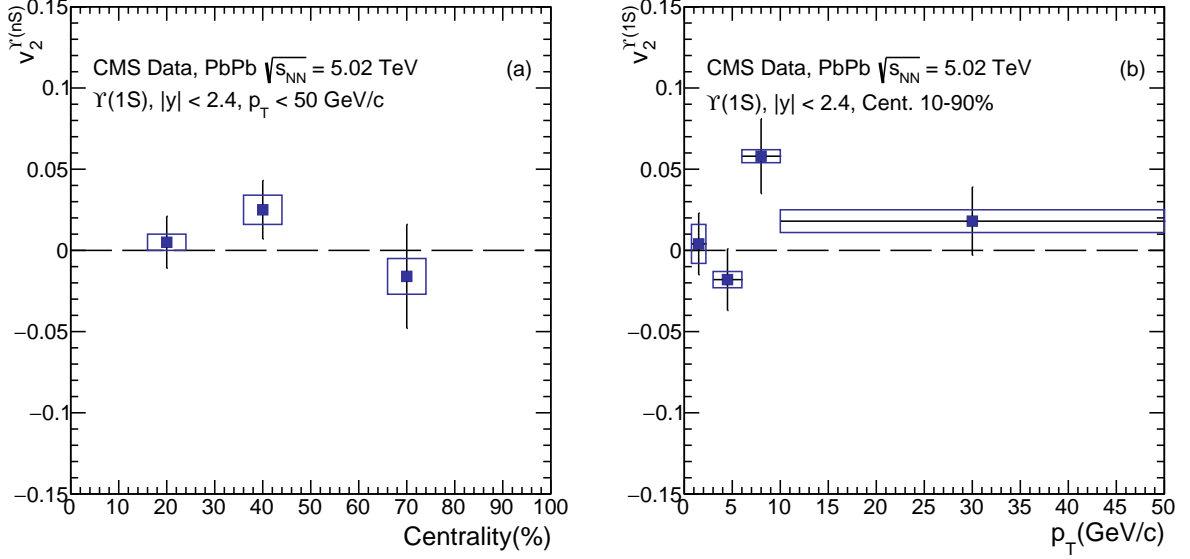
Figure 8: (Color online) The Υ(1S) azimuthal anisotropy (v_2) (a) as a function of collision centrality and (b) as a function of transverse momentum p_T [82]. The vertical bars denote statistical uncertainties, and the rectangular boxes show the total systematic uncertainties.

Υ(1S) meson v_2 values is measured for the 10-90% centrality interval. The v_2 values are consistent with zero in the measured p_T range, except for the 6<p_T <10 GeV/c interval that shows a 2.6σ deviation from zero.

Figure 9 shows the p_T differential results for v_2 of Υ(1S) mesons measured by CMS experiment along with the measurements of v_2 for Υ(1S) and J/ψ from ALICE in the same p_T (0-15 GeV/c) and centrality (5-60%) interval. The measurements from CMS and ALICE are done in complementary rapidity ranges. The Υ(1S) V_2 is consistant with zero while the J/ψ meson measured by ALICE in same kinematic conditions have finite v_2. Together, the CMS and ALICE results indicate that the geometry of the medium has little influence on the Υ(1S) yields and recombination is not a dominant process in the production of this meson. The results also indicate that the path-length dependence of Υ(1S) suppression is small.

4.3. Υ(nS) R_{pA}

CMS measured the $Upsilon$ ratios as a function of event activity measured in in $\sqrt{s_{NN}}$=5.02 TeV pPb [84] and compared with $\sqrt{s}$=2.76 TeV pp and PPb Collisions. The nuclear modification of all Υ states is also measured in pPb collisions at $\sqrt{s_{NN}}$ = 5.02 TeV [85]. Recently, relative production of Υ(nS) states are measured as a function of event activity in proton-proton collisions at $\sqrt{s}$ = 7 TeV [86]

Figure 10(a) shows the ratio Υ(2S)/Υ(1S) as a function of event activity measured in $\sqrt{s_{NN}}$=5.02 TeV pPb collisions [84] and is compared with pp and PbPb Collisions at $\sqrt{s_{NN}}$=2.76 TeV. Figure 10(b) shows the Υ(nS) nuclear modification factor, R_{AA} as a function of N_{Part} at $\sqrt{s_{NN}}$=5.02 TeV measured by CMS [77].

The N_{tracks} corresponding to N_{Part} in Fig 10 at 5.02 TeV can be obtained using the N_{tracks} for same N_{Part} given for 2.76 TeV [76] and scale as

$$N_{\mathrm{tracks}}|_{5.02} = N_{\mathrm{tracks}}|_{2.76} \times \frac{dN/d\eta|_{5.02}}{dN/d\eta|_{2.76}}. \tag{5}$$
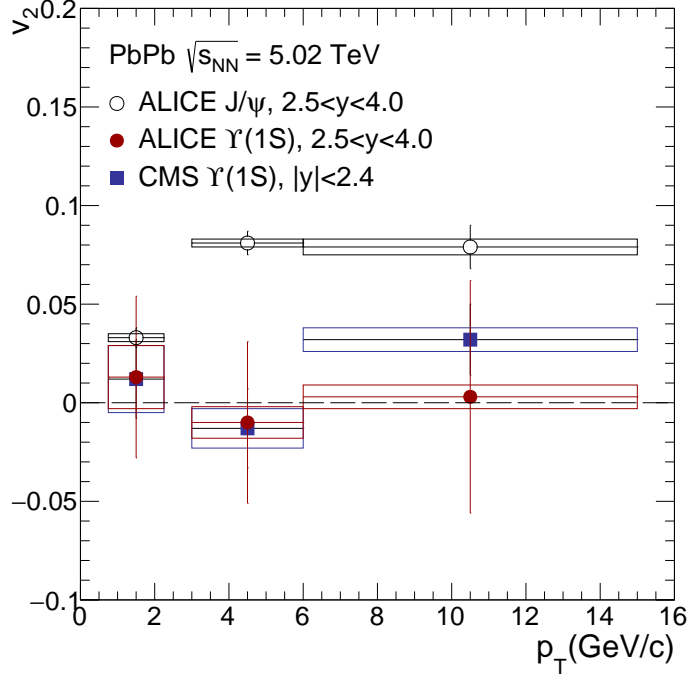
18

Figure 9: (Color online) The v$_2$ for Υ(1S) mesons as a function of p$_T$ in the rapidity range $|y| < 2.4$ measured by CMS experiment [82] compared with the ALICE results for $Upsilon$(1S) and J/ψ mesons measured in 2.5<y<4 [83]. The vertical bars denote statistical uncertainties, and the rectangular boxes show the total systematic uncertainties.
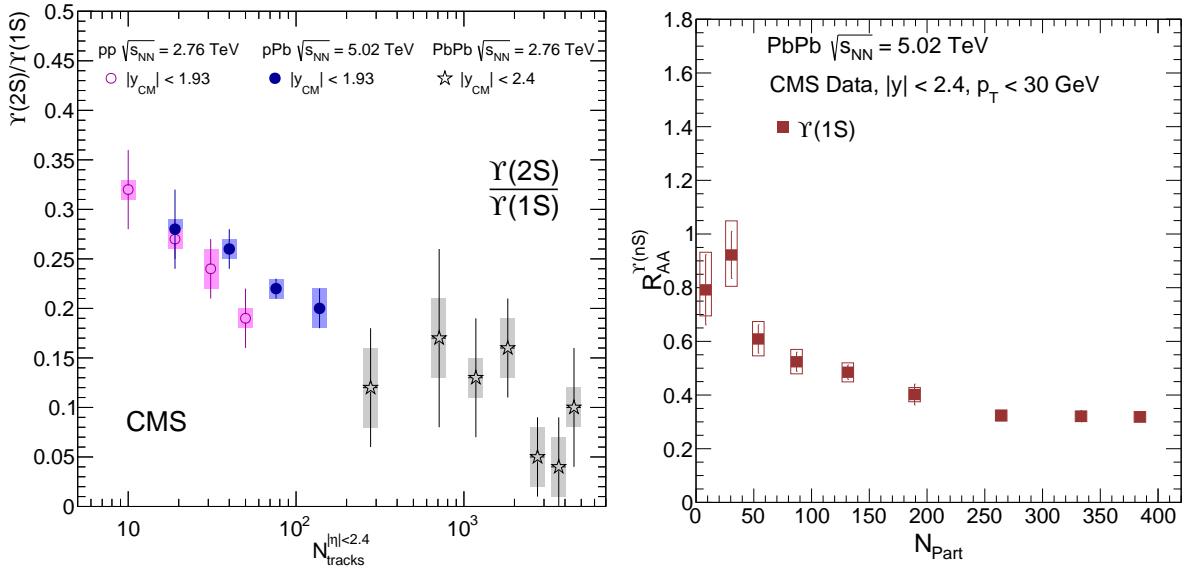

Figure 10: (Color online) (a) The ratio Υ(2S)/Υ(1S) as a function of event activity measured in $\sqrt{s_{NN}}$=5.02 TeV pPb collisions [84] and is compared with pp and PbPb Collisions at $\sqrt{s_{NN}}$=2.76 TeV. (b) The Υ(nS) nuclear modification factor, R_{AA} as a function of N_{Part} at $\sqrt{s_{NN}}$=5.02 TeV measured by CMS [77].
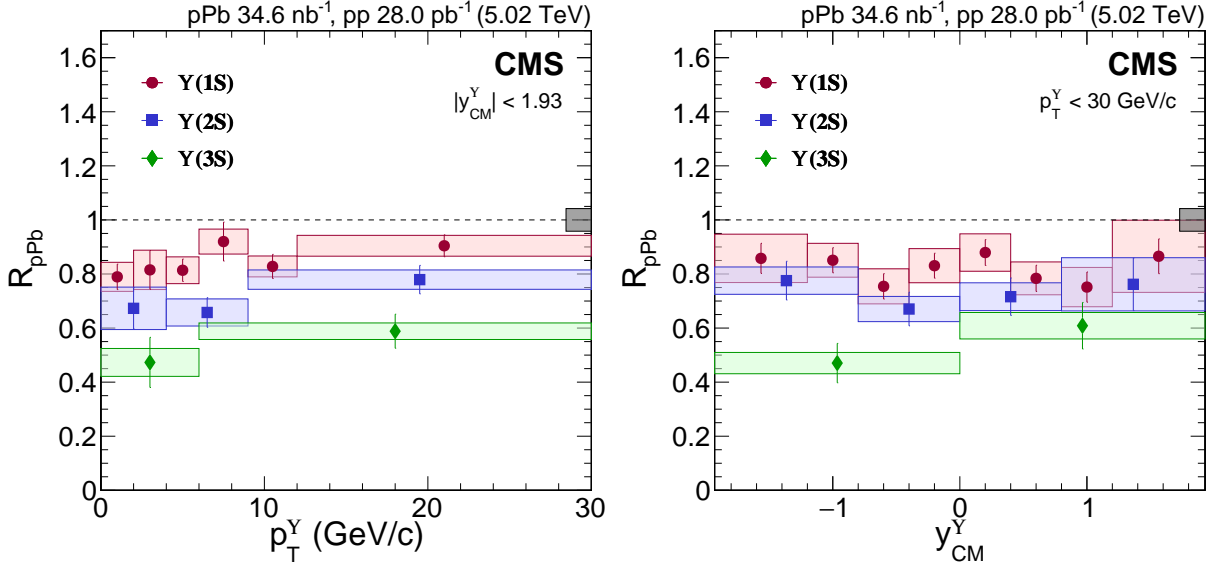
Figure 11: (Color online) The Υ(nS) nuclear modification factor, R_{pA}, (a) as a function of transverse momentum p_T and (b) as a function rapidity in pPb colisions at 5.02 TeV measured by CMS [85]

where $\frac{dN/d\eta|_{5.02}}{dN/d\eta|_{2.76}}$.

The ratio Υ(2S)/Υ(1S) at $\sqrt{s_{NN}}$=5.02 can be obtained as

$$\frac{\Upsilon(2S)}{\Upsilon(1S)} = \frac{R_{AA}^{2S}}{R_{AA}^{1S}} \times \frac{\sigma_{pp}^{1S}}{\sigma_{pp}^{2S}}. \tag{6}$$

Here σ_{pp}^{1S} and σ_{pp}^{2S} can be obtained by integrating the pp cross section measured by CMS [77].

5. Bottomonia production mechanism in heavy ion collisions

Quarkonia production in nuleus-nucleus (A-A) collisions became a vibrant area of research after the seminal paper of Matsui and Satz [4]. It was proposed that quarkonium production would be suppressed compared to the same in the case of p-p collisions. Such a suppression, as proposed, would be a signature of the formation of the QGP phase as the in that phase the strong force would be colour screened. As a result the binding between the heavy quark pairs would be significantly weakened leading to the melting of the corresponding bound states.

However, very soon it was revealed that the picture was not that simple. There are many factors which affect the production of quarkonia in A-A collisions. In fact, quarkonium suppression was also observed in proton-nucleus (pA) collisions, so that part of the nucleus-nucleus suppression is due to cold-nuclear-matter effects. Therefore it is necessary to disentangle hot and cold-medium effects. The CNM effect has mainly two sources : the initial state modification and the final state modification. The initial state modification arises due to modification of parton distribution functions (PDF) inside the nucleus compared to the same inside the protons. The final state modification arises due to the fact the produced quarkonia has to interact with the medium leading to the destabilisation of the bound state. Furthermore, the suppression of quarkonia is thought to be of sequential in nature. The sequential suppression happens as a result of the differences of the binding energy of different bound states. The strongly bound states, such as the Υ(1S) or the J/ψ , melt at higher temperatures. On the other hand more loosely bound staes ψ(2S) , χ_c ,
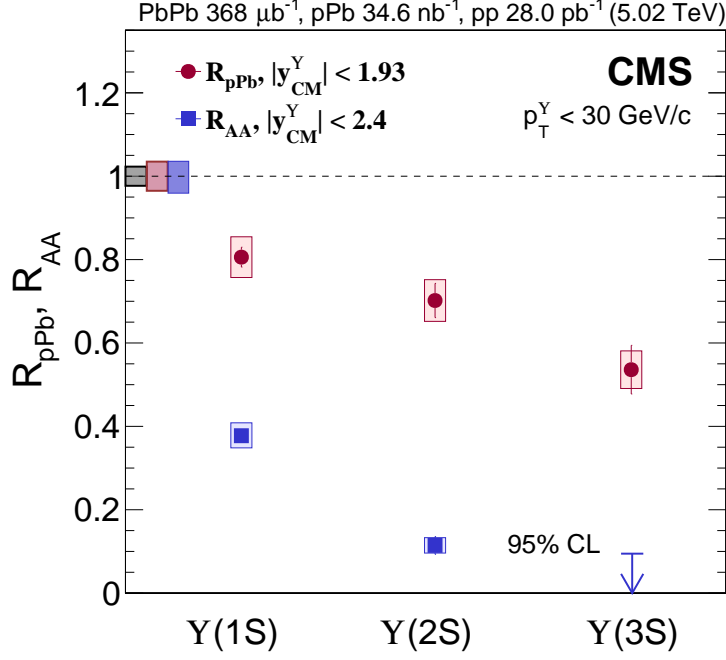
Figure 12: (Color online) The Υ(nS) nuclear modification factors, R_{pA} [85] and R_{AA} [77] at 5.02 TeV measured by CMS.

χ_b, Υ(2S) or Υ(3S) melt at much lower temperatures. This issue throws light towards the estimate of the initial temperature reached in the collisions [87]. However, the prediction of a sequential suppression pattern is complicated feed-down decays of higher-mass resonances and other issues. The production process is further complicated, in the high energy scenario (like LHC), by recombination mechanics. At very high energies abundant production of Q and $\bar{Q}$ may lead to new quarkonia production source. However, this production process is mainly observed in charm quarks and hence in charmonium states. Bottom quarks, being very heavy, do not show any significant recombination effect even in top LHC energies.

To quantify the effect of medium in the quarkonia production scenario one takes recourse to a quantity called the nuclear modification factor (R_{AA}). This quantity is defined as the ratio of the quarkonium yield in the A-A collisions to the same in case of p-p collisions scaled by the number of collisions :

$$R_{AA} = \frac{1}{\langle N_{coll} \rangle} \frac{N_{AA}^{Q\bar{Q}}}{N_{pp}^{Q\bar{Q}}} \tag{7}$$

The ratio will be unity if the physics of the A-A collisions is simply the sum of a large number p-p collisions. The effect of the medium should make it vary from unity.

5.1. Quarkonium in hot medium

It has been argued that color screening in a deconfined QCD medium will destroy $Q\overline{Q}$ bound states at sufficiently high temperatures. The binding of heavy quarks depend on the screening radius (r_D). If the binding radius of the heavy quark bound state (r_Q) is is much greater than the screening radius radius then the one heavy quark gets screened from the other and the pair becomes unstable to binding. The screening radius is inversely proportional to

the temperature. As the temperature increases the screening radius becomes smaller and smaller compared to the binding radius and the quarkonium states become more and more unstable. Although this idea was proposed long ago, first principle QCD calculations, which go beyond qualitative arguments, have been performed more recently. Such calculations include lattice QCD determinations of quarkonium correlators [88, 89, 90, 91, 92], potential model calculations of the quarkonium spectral functions with potentials based on lattice QCD [87, 93, 94, 95, 96, 97, 98, 99], as well as effective field theory approaches that justify potential models and reveal new medium effects [100, 101, 102, 103]. Furthermore, better modeling of quarkonium production in the medium created by heavy-ion collisions has been achieved. These advancements make it possible to disentangle the cold and hot-medium effects on the quarkonium states, crucial for the interpretation of heavy-ion data.
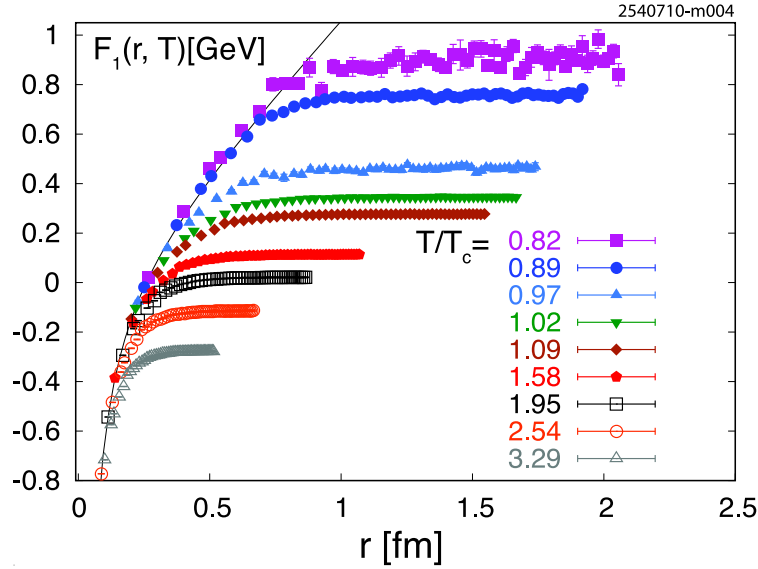

Figure 13: Heavy-quark-singlet free energy versus quark separation calculated in 2+1 flavour QCD on $16^3 \times 4$ lattices at different temperatures [104, 105]

Color screening is studied on the lattice by calculating the spatial correlation function of a static quark and antiquark in a color-singlet state which propagates in Euclidean time from $\tau = 0$ to $\tau = 1/T$, where T is the temperature. Lattice calculations of this quantity with dynamical quarks have been reported [106, 104, 105]. The logarithm of the singlet correlation function, also called the singlet free energy, is shown in Fig. 13. As expected, in the zero-temperature limit the singlet free energy coincides with the zero-temperature potential. Figure 13 also illustrates that, at sufficiently short distances, the singlet free energy is temperature independent and equal to the zero-temperature potential. The range of interaction decreases with increasing temperature. For temperatures above the transition temperature, T_c, the heavy-quark interaction range becomes comparable to the charmonium radius. Based on this general observation, one would expect that the charmonium states, as well as the excited bottomonium states, do not remain bound at temperatures just above the deconfinement transition, often referred to as dissociation or melting.

In-medium quarkonium properties are encoded in the corresponding spectral functions, as is quarkonium dissociation at high temperatures. Spectral functions are defined as the imaginary part of the retarded correlation function of
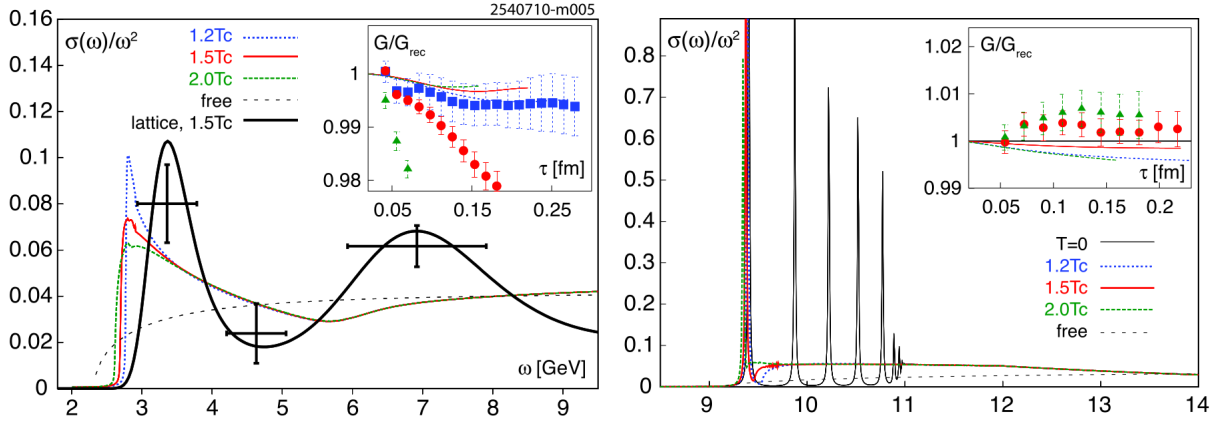
Figure 14: The S-wave charmonium (a) and bottomonium (b) spectral functions calculated in potential models. Insets: correlators compared to lattice data. The *dotted curves* are the free spectral functions. Figure is taken from Ref. [98].

Table 9: Upper bounds on the dissociation temperatures [99].

State	$\chi_{cJ}(1P)$	ψ'	J/ψ	$\Upsilon(2S)$	$\chi_{bJ}(1P)$	$\Upsilon(1S)$
T_{diss}	$\leq T_c$	$\leq T_c$	$1.2T_c$	$1.2T_c$	$1.3T_c$	$2T_c$

quarkonium operators. Bound states appear as peaks in the spectral functions. The peaks broaden and eventually disappear with increasing temperature. The disappearance of a peak signals the melting of the given quarkonium state. The quarkonium spectral functions can be calculated in potential models using the singlet free energy from Fig. 13 or with different lattice-based potentials obtained using the singlet free energy as an input [98, 99]. The results for quenched QCD calculations are shown in Fig. 14 for S-wave charmonium (a) and bottomonium (b) spectral functions [98]. All charmonium states are dissolved in the deconfined phase while the bottomonium 1S state may persist up to $T \sim 2T_c$. An upper bound on the dissociation temperature (the temperatures above which no bound states peaks can be seen in the spectral function and bound state formation is suppressed) can be obtained from the analysis of the spectral functions. Conservative upper limits on the dissociation temperatures for the different quarkonium states obtained from a full QCD calculation [99] are given in Table 9.

Potential model calculations based on lattice QCD, as well as resummed perturbative QCD calculations, indicate that all charmonium states and the excited bottomonium states dissolve in the deconfined medium. This leads to the reduction of the quarkonium yields in heavy-ion collisions compared to the binary scaling of pp collisions. Recombination and edge effects, however, guarantee a nonzero yield.

5.2. Cold nuclear matter effects

The baseline for quarkonium production and suppression in heavy-ion collisions should be determined from studies of cold-nuclear-matter (CNM) effects. The name cold matter arises because these effects are observed in hadron-nucleus interactions dense matter effects are much more important compared to the hot matter. There are several CNM effects. The first such effect is the modifications of the parton distribution functions (PDF) in the

nucleus compared to that in the nucleon. It depends mainly on two parameters, the momentum fraction of the parton (x) and the scale of the parton-parton interaction (Q^2). The nuclear density modified parton distributed function is known as nPDF. The nPDF to PDF ratio throws light on the modification quarkonia production in the CNM due to the modification of PDFs. This quantity is denoted as $R_i(x, Q^2) = f_i^{p \epsilon A}(x, Q^2)/f_i^p(x, Q^2)$. In the small x regime $(x < 10^{-2})$ this ration is less than unity. This feature is referred to as small-x shadowing. At intermediate x (~ 0.1) the ratio shows a hump like structure a phenomenon known as anti-shadowing. Around $x \approx 0.6$ one observes a dip which is known as EMC effect. The dynamics of partons within the nuclei is affected by the parton saturation which is successfully studied by color glass condensate. In the final state the quarkonia bound state scatter and re-scatter inelastically while passing through the nucleus. This leads the breakup or absorption of the bound state which is estimated by the inelastic cross-section of the quarkonia with the nucleon.

Even though the contributions to CNM effects may seem rather straightforward, there are a number of associated uncertainties. First, while nuclear modifications of the quark densities are relatively well-measured in nuclear deep-inelastic scattering (nDIS), the modifications of the gluon density are not directly measured. The nDIS measurements probe only the quark and antiquark distributions directly. The scaling violations in nDIS can be used to constrain the nuclear gluon density. Overall momentum conservation provides another constraint. However, more direct probes of the gluon density are needed. Current shadowing parametrizations are derived from global fits to the nuclear parton densities and give wide variations in the nuclear gluon density, from almost no effect to very large shadowing at low-x, compensated by strong antishadowing around $x \sim 0.1$.

The nuclear absorption survival probability depends on the quarkonium absorption cross section. There are more inherent uncertainties in absorption than in the shadowing parametrization. It is obtained from data on other processes and is independent of the final state. Typically an absorption cross section is fit to the A dependence of J/ψ and/or ψ' production in pA collision at a given energy. This is rather simplistic since it is unknown whether the object traversing the nucleus is a precursor color-octet state or a fully-formed color-singlet quarkonium state. The J/ψ absorption cross section at $y \sim 0$ is seen to decrease with energy, regardless of the chosen shadowing parametrization [107].

Recent analyses of J/ψ production in fixed-target interactions [107] show that the effective absorption cross section depends on the energy of the initial beam and the rapidity or x_F of the observed J/ψ . One possible interpretation is that low-momentum color-singlet states can hadronize in the target, resulting in larger effective absorption cross sections at lower center-of-mass energies and backward x_F (or center-of-mass rapidity). At higher energies, the states traverse the target more rapidly so that the x_F values at which they can hadronize in the target move back from midrapidity toward more negative x_F. Finally, at sufficiently high energies, the quarkonium states pass through the target before hadronizing, resulting in negligible absorption effects. Thus the *effective* absorption cross section decreases with increasing center-of-mass energy because faster states are less likely to hadronize inside the target.

This is a very simplistic picture. In practice, cold-nuclear-matter effects (initial-state energy loss, shadowing, final-state breakup, *etc.*) depend differently on the quarkonium kinematic variables and the collision energy. It is clearly unsatisfactory to combine all these mechanisms into an *effective* absorption cross section, as employed in the Glauber formalism, that only evaluates final-state absorption. Simply taking the σ_{abs} obtained from the analysis of the pA data and using it to define the Pb+Pb baseline is not be sufficient. A better understanding of absorption requires more detailed knowledge of the production mechanisms which it self are largely unknown.

5.3. Kinetic approach

In the kinetic approach [108], the proper time τ evolution of the quarkonia population N_Q is given by the rate equation

$$\frac{dN_Q}{d\tau} = -\lambda_D \rho_g N_Q + \lambda_F \frac{N_{q\bar{q}}^2}{V(\tau)}, \tag{8}$$

where $V(\tau)$ is the volume of the deconfined spatial region and $N_{q\bar{q}}$ is the number of initial heavy quark pairs produced per event depending on the centrality defined by the number of participants N_{part}. The λ_D is the dissociation rate obtained by the dissociation cross section averaged over the momentum distribution of gluons and λ_F is the formation rate obtained by the formation cross section averaged over the momentum distribution of heavy quark pair q and $\bar{q}$. ρ_g is the density of thermal gluons. The number of quarkonia at freeze-out time τ_f is given by the solution of Eq. (8),

$$N_Q(p_T) = S(p_T)\, N_Q^{\text{PbPb}}(p_T) + N_Q^F(p_T). \tag{9}$$

Here $N_Q^{\text{PbPb}}(p_T)$ is the number of initially-produced quarkonia (including shadowing) as a function of p_T and $S(p_T)$ is their survival probability from gluon collisions at freeze-out,

$$S(p_T) = \exp\left(-\int_{\tau_0}^{\tau_f} f(\tau)\lambda_D(T, p_T)\,\rho_g(T)\,d\tau\right). \tag{10}$$

The temperature $T(\tau)$ and the QGP fraction $f(\tau)$ evolve from initial time τ_0 to freeze-out time τ_f due to expansion of the QGP. The initial temperature and the evolution is dependent on collision centrality N_{part}. $N_Q^F(p_T)$ is the number of regenerated quarkonia per event,

$$N_Q^F(p_T) = S(p_T)N_{q\bar{q}}^2 \int_{\tau_0}^{\tau_f} \frac{\lambda_F(T, p_T)}{V(\tau)\, S(\tau, p_T)} d\tau. \tag{11}$$

The nuclear modification factor (R_{AA}) can be written as

$$R_{AA}(p_T) = S(p_T)\, R(p_T) + \frac{N_Q^F(p_T)}{N_Q^{pp}(p_T)}. \tag{12}$$

Here $R(p_T)$ is the shadowing factor.

In the color dipole approximation, the gluon dissociation cross section as function of gluon energy, q^0, in the quarkonium rest frame is [109]

$$\sigma_D(q^0) = \frac{8\pi}{3} \frac{16^2}{3^2} \frac{a_0}{m_q} \frac{(q^0/\epsilon_0 - 1)^{3/2}}{(q^0/\epsilon_0)^5}, \tag{13}$$

where ϵ_0 is the quarkonia binding energy and m_q is the charm/bottom quark mass and $a_0 = 1/\sqrt{m_q \epsilon_0}$. The values of ϵ_0 are taken as 0.64 and 1.10 GeV for the ground states, J/ψ and $\Upsilon(1S)$, respectively [110]. For the first excited state of bottomonia, $\Upsilon(2S)$, we use dissociation cross section from Ref. [111].

Figure 15 shows the gluon dissociation cross sections of J/ψ and $\Upsilon(1S)$ as a function of gluon energy. The dissociation cross section is zero when the gluon energy is less than the binding energy of the quarkonia. It increases with gluon energy and reaches a maximum at 1.2 (1.5) GeV for J/ψ ($\Upsilon(1S)$). At higher gluon energies, the interaction probability decreases. The gluon energy q^0 is related to the square of the center of mass energy s, of the quarkonium-gluon system by

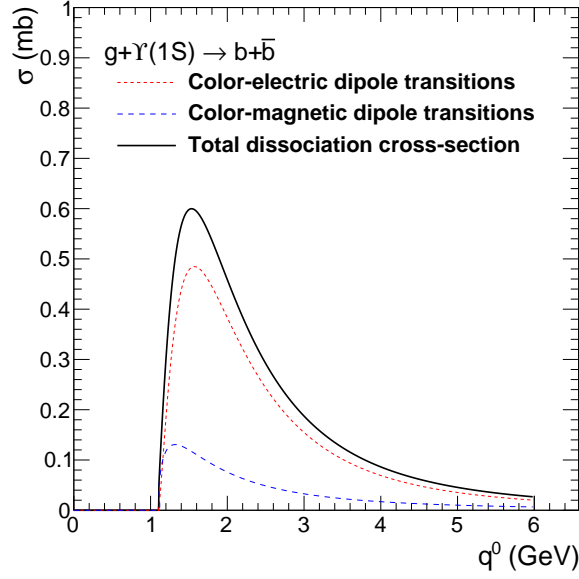$$q^0 = \frac{s - M_Q^2}{2\, M_Q} \tag{14}$$

25

Figure 15: (Color online) Gluon dissociation cross section of quarkonia as a function of gluon energy (q^0) in quarkonia rest frame.

where M_Q ais the mass of quarkonium. We calculate the dissociation rate as a function of quarkonium momentum by integrating the dissociation cross section over thermal gluon momentum distribution $f_g(p_g)$.

We can calculate the formation cross section from the dissociation cross section using detailed balance [108, 112],

$$\sigma_F = \frac{48}{36}\,\sigma_D(q^0)\frac{(s - M_Q^2)^2}{s(s - 4m_q^2)}. \tag{15}$$

The formation rate of quarkonium with momentum **p** can be obtained using thermal distribution functions of $q/\bar{q}$.

Figure 16(a) and (b) show the calculations of contributions to the nuclear modification factor, R_{AA}, for the Υ(1S) and Υ(2S) respectively as a function of p_T compared with the mid rapidity measurements from CMS [8]. The gluon dissociation mechanism combined with the pion dissociation and shadowing corrections gives good description of data in mid p_T range ($p_T \approx$ 5-10 GeV/c) for both Υ(1S) and Υ(2S). The contribution from the regenerated Υs is negligible even at LHC energies. Our calculations under-predict the suppression observed at the highest measured p_T for Υ(1S) and Υ(2S) which is similar for the case of J/ψ. The states Υ(1S) and Υ(2S) also have feed-down contributions from decays of higher b$\bar{\text{b}}$ bound states. The nuclear modification factor, R_{AA} is obtained taking into account the feed-down corrections as follows

$$R_{AA}^{\Upsilon(3S)} = R_{AA}^{\Upsilon(3S)} \tag{16}$$

$$R_{AA}^{\Upsilon(2S)} = f_1 R_{AA}^{\Upsilon(2S)} + f_2 R_{AA}^{\Upsilon(3S)} \tag{17}$$

$$R_{AA}^{\Upsilon(1S)} = g_1 R_{AA}^{\Upsilon(1S)} + g_2 R_{AA}^{\chi_b(1P)} + g_3 R_{AA}^{\Upsilon(2S)} + g_4 R_{AA}^{\Upsilon(3S)} \tag{18}$$

The factors f's and g's are obtained from CDF measurement [113]. The values of g_1, g_2, g_3 and g_4 are 0.509, 0.27, 0.107 and 0.113 respectively. Here g_4 is assumed to be the combined fraction of Υ(3S) and χ_b(2P). The values of f_1
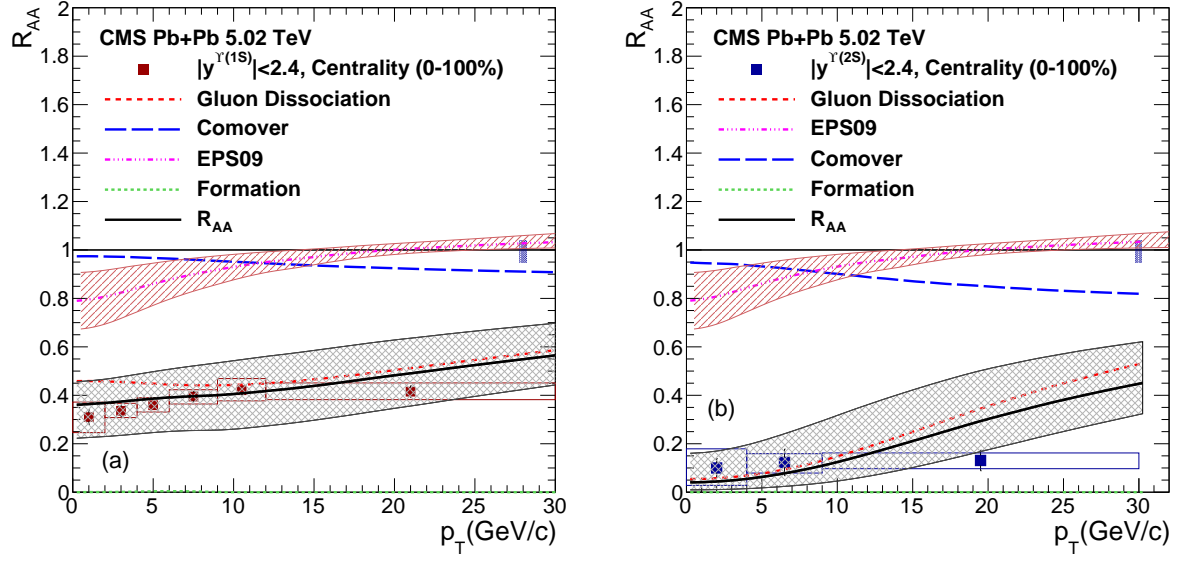
Figure 16: (Color online) Calculated nuclear modification factor (R_{AA}) of (a) Υ(1S) and (b) Υ(2S) as a function of p_T compared with CMS measurements [8]. The global uncertainty in R_{AA} is shown as a band around the line at 1.
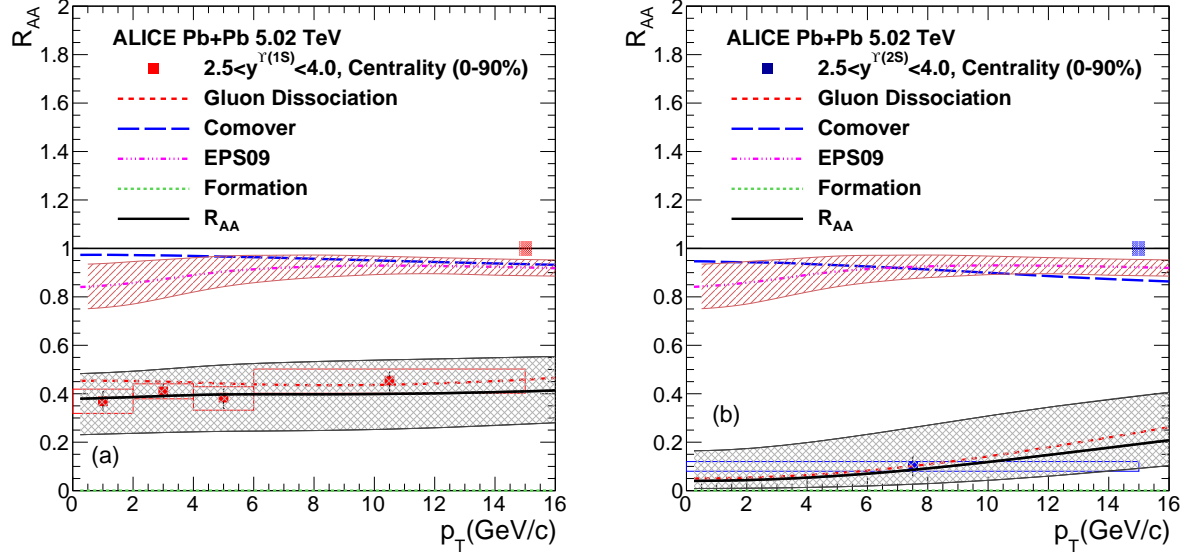

Figure 17: (Color online) Calculated nuclear modification factor (R_{AA}) of (a) Υ(1S) and (b) Υ(2S) as a function of p_T in the kinematic range of ALICE detector at LHC [78]. The global uncertainty in R_{AA} is shown as a band around the line at 1.
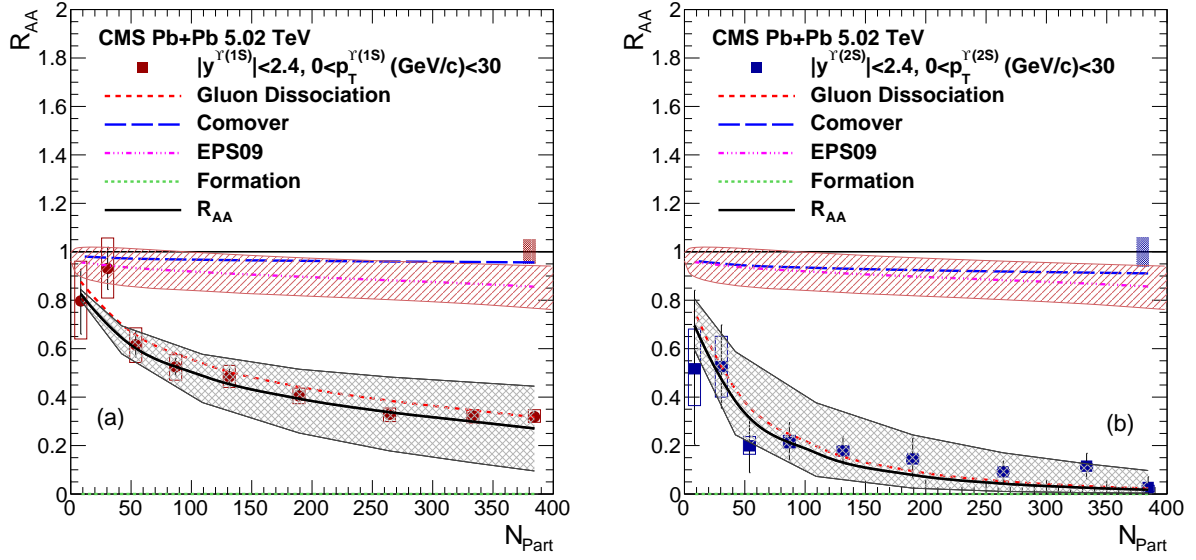
Figure 18: (Color online) Calculated nuclear modification factor (R_{AA}) of (a) Υ(1S) and (b) Υ(2S) as a function of centrality of the collisions compared with the CMS measurements [8]. The global uncertainty in R_{AA} is shown as a band around the line at 1.

and f_2 are taken as 0.50 [114].

Figure 17(a) and (b) show the model prediction of the nuclear modification factor, R_{AA}, for the Υ(1S) and Υ(2S) respectively as a function of p_T in the kinematic range covered by ALICE detector. The ALICE data [78] is well described by our model.

Figure 18(a) depicts the calculated centrality dependence of the Υ(1S) nuclear modification factor, along with the midrapidity data from CMS [8]. Our calculations combined with the pion dissociation and shadowing corrections gives very good description of the measured data. Figure 18(b) shows the same for the Υ(2S) along with the midrapidity CMS measurements. The suppression of the excited Υ(2S) states is also well described by our model. As stated earlier, the effect of regeneration is negligible for Υ states.

The suppression of quarkonia by comoving pions can be calculated by folding the quarkonium-pion dissociation cross section $\sigma_{\pi Q}$ over thermal pion distributions [115]. It is expected that at LHC energies, the comover cross section will be small [107]. The pion-quarkonia cross section is calculated by convoluting the gluon-quarkonia cross section σ_D over the gluon distribution inside the pion [111],

$$\sigma_{\pi Q}(p_\pi) = \frac{p_+^2}{2(p_\pi^2 - m_\pi^2)} \int_0^1 dx\, G(x)\, \sigma_D(xp_+/\sqrt{2}), \qquad (19)$$

where $p_+ = (p_\pi + \sqrt{p_\pi^2 - m_\pi^2})/\sqrt{2}$. The gluon distribution, $G(x)$, inside a pion is given by the GRV parameterization [116]. The dissociation rate λ_{D_π} can be obtained using the thermal pion distribution.

5.4. Transport approach in bottomonia production

There have been some studies in looking at the transport approach to the bottomonia production. [117, 118]. This is an approach of studying the rate equations. Such an equation for bottomonium production in the medium's rest frame can be written as [117],

$$\frac{dN_Y(\tau)}{d\tau} = -\Gamma_Y(T)\left[N_Y(\tau) - N_Y^{\mathrm{eq}}(T)\right], \qquad (20)$$
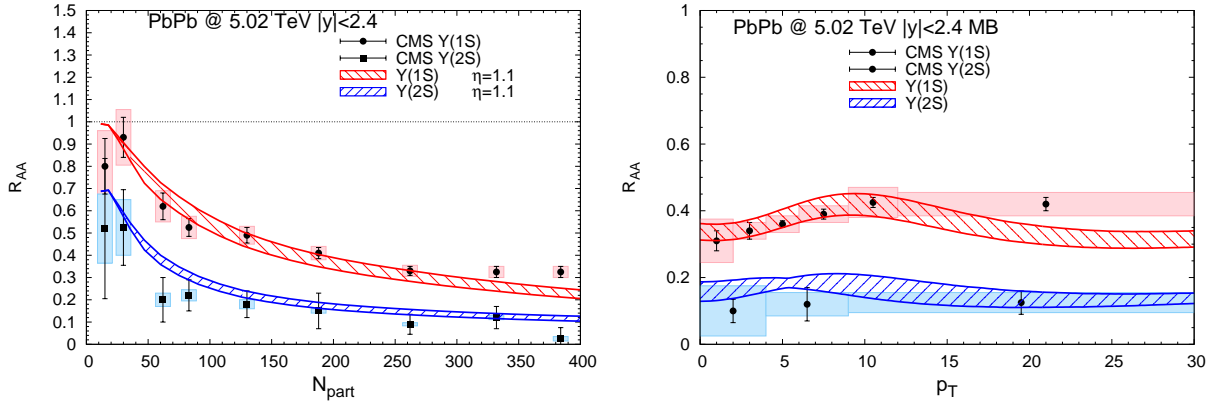
Figure 19: Centrality (left) and transverse-momentum (right) dependence of the R_{AA} for $\Upsilon(1S)$ and $\Upsilon(2S)$ in 5.02 TeV Pb-Pb collisions at the LHC, compared to CMS data [120]. The bands represent a 0-15 % shadowing [50] on open-bottom and bottomonia.

In the above equation Γ_Y, is the inelastic reaction rate and $N_Y^{\mathrm{eq}}(T)$ is the thermal equilibrium limit for each state $Y = \Upsilon(1S), \Upsilon(2S), \chi_c, ...$

In the reaction rates both gluo-dissociation and quasi-free mechanisms have been incorporated. An important ingredient in this calculation is the bottomonium binding energies. The thermal-equilibrium limit is evaluated from the statistical model with bottom (b) quarks [119]. The initial conditions are obtained from the pp collision data. With these inputs the study is carried out in a hydrodynamicaly expanding scenario.

Figure 19 shows the results contrasted with the mid-rapidity data of STAR (at $\sqrt{s}$=200 GeV) [121] and CMS (at $\sqrt{s}$=5.02 TeV) [120], respectively. The authors of this model found a reasonable agreement with experimental data for the centrality dependence of both $\Upsilon(1S)$ and $\Upsilon(2S)$ at both collision energies. Interestingly they could reproduce the strong suppression of the $\Upsilon(2S)$ observed by STAR. The calculated p_T spectra at 5.02 TeV appear to capture the rather flat shapes in the CMS data.

5.5. Suppression in anisotropic medium

In a series of papers [114, 122, 123] people have studied bottomonia suppression using anisotropic hydrodynamics. There are two major *new* ingredients to this work : (1) the first-principles calculation of the thermal widths of heavy quarkonium states and (2) consideration of the momentum anisotropy of the plasma.

In these works the phase-space distribution of gluons in the local rest frame is assumed to be

$$f(\mathbf{x}, \mathbf{p}) = f_{\mathrm{iso}}\left(\sqrt{\mathbf{p}^2 + \xi(\mathbf{p} \cdot \mathbf{n})^2}/p_{\mathrm{hard}}\right) \tag{21}$$

In the above equation ξ is a measure of the degree of anisotropy of the plasma given as $\xi = \frac{1}{2}\langle \mathbf{p}_\perp^2 \rangle / \langle p_z^2 \rangle - 1$ where p_z and $\mathbf{p}_\perp$ are the partonic longitudinal and transverse momenta in the local rest frame, respectively. In equation 21, p_{hard} is the momentum scale of the particles and can be identified with the temperature in an isotropic plasma.

An approximate form of the real perturbative heavy quark potential as function of ξ can be written as [124] (for

$N_c = 3$ and $N_f = 2$).

$$
\begin{aligned}
Re[V_{\text{pert}}] &= -\alpha \exp(-\mu r)/r \\
\left(\frac{\mu}{m_D}\right)^{-4} &= 1 + \xi \left(1 + \frac{\sqrt{2}(1+\xi)^2 \left(\cos(2\theta) - 1\right)}{(2+\xi)^{5/2}} \right)
\end{aligned}
\tag{22}
$$

where $\alpha = 4\alpha_s/3$, $m_D^2 = (1.4)^2 16\pi\alpha_s p_{\text{hard}}^2/3$ is the isotropic Debye mass and θ is the angle with respect to the beamline. The factor of $(1.4)^2$ accounts for higher-order corrections to the isotropic Debye mass [125].

This perturbative potential, given in equation (21) is modified to include the non-perturbative (long range) contributions. The modified real part of the potential is given as [124]

$$
Re[V] = -\frac{\alpha}{r} \left(1 + \mu r\right) \exp\left(-\mu r\right) + \frac{2\sigma}{\mu} \left[1 - \exp\left(-\mu r\right)\right] - \sigma r \, \exp(-\mu r) - \frac{0.8\,\sigma}{m_Q^2\, r}\,,
\tag{23}
$$

where the last term is a temperature- and spin-independent quark mass correction [126] and $\sigma = 0.223$ GeV is the string tension. Here α is chosen to be 0.385 to match zero temperature binding energy data for heavy quark states [124]. The imaginary part of the potential is taken as the same as the perturbative heavy quark potential up to linear order in ξ

$$
Im[V_{\text{pert}}] = -\alpha p_{\text{hard}} \left\{ \phi(\hat{r}) - \xi \left[\psi_1(\hat{r}, \theta) + \psi_2(\hat{r}, \theta)\right] \right\},
\tag{24}
$$

where $\hat{r} = m_D r$ and ϕ, ψ_1, and ψ_2 are defined in Ref. [122].

The full model potential, given by $V = Re[V] + iIm[V]$, is used to solve the Schrödinger equation. Solution of the Schrödinger equation gives the real and imaginary parts of the binding energy of the states. The imaginary part defines the instantaneous width of the state $Im[E_{\text{bind}}(p_{\text{hard}}, \xi)] \equiv -\Gamma_T(p_{\text{hard}}, \xi)/2$. The resulting width $\Gamma_T(\tau)$ implicitly depends on the initial temperature of the system.

The following rate equation is used to account for in-medium bottomonia state decay,

$$
\frac{dn(\tau, \mathbf{x}_\perp, \varsigma)}{d\tau} = -\Gamma(\tau, \mathbf{x}_\perp, \varsigma) n(\tau, \mathbf{x}_\perp, \varsigma),
\tag{25}
$$

where $\tau = \sqrt{t^2 - z^2}$ is the longitudinal proper time, $\mathbf{x}_\perp$ is the the transverse coordinate and $\varsigma = \operatorname{arctanh}(z/t)$ is the the spatial rapidity. The rate of decay is computed by [114]

$$
\begin{aligned}
\Gamma(\tau, \mathbf{x}_\perp, \varsigma) &= 2Im[E_{\text{bind}}(\tau, \mathbf{x}_\perp, \varsigma)] & Re[E_{\text{bind}}(\tau, \mathbf{x}_\perp, \varsigma)] > 0 \tag{26} \\
&= \gamma_{\text{dis}} & Re[E_{\text{bind}}(\tau, \mathbf{x}_\perp, \varsigma)] \leq 0. \tag{27}
\end{aligned}
$$

In order to look at the suppression one has to calculate R_{AA}. The algorithm to obtain R_{AA} is the following. First one obtains

$$
\bar{\gamma}(\mathbf{x}_\perp, p_T, \varsigma, b) \equiv \Theta(\tau_f - \tau_{\text{form}}(p_T)) \int_{\max(\tau_{\text{form}}(p_T), \tau_0)}^{\tau_f} d\tau\, \Gamma_T(\tau, \mathbf{x}_\perp, \varsigma, b)
\tag{28}
$$

where ς is the spatial rapidity. From this one obtains

$$
R_{AA}(\mathbf{x}_\perp, p_T, \varsigma, b) = \exp(-\bar{\gamma}(\mathbf{x}_\perp, p_T, \varsigma, b))
\tag{29}
$$

Finally, one averages over $\mathbf{x}_\perp$ to obtain

$$
\langle R_{AA}(p_T, \varsigma, b) \rangle \equiv \left[\int_{\mathbf{x}_\perp} d\mathbf{x}_\perp\, T_{AA}(\mathbf{x}_\perp)\, R_{AA}(\mathbf{x}_\perp, p_T, \varsigma, b)\right] / \left[\int_{\mathbf{x}_\perp} d\mathbf{x}_\perp\, T_{AA}(\mathbf{x}_\perp)\right]
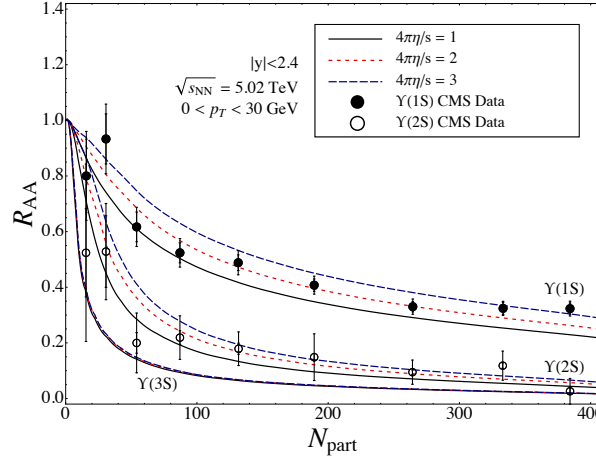\tag{30}
$$

Figure 20: Calculation for the inclusive $\Upsilon(nS)$ curves as a function of N_{part}. A comparison is made for the CMS experiment at the LHC.

In Fig. 20 the R_{AA} for $\Upsilon(1s)$ and χ_{b1} has been plotted as a function of N_{part}. The authors have depicted that there is substantial suppression of $\Upsilon(1s)$ which they have accounted to the in-medium decay. A similar suppression pattern is observed for χ_{b1}. This may be attributed to the finite formation time of the χ_{b1}.

6. Summary and Conclusions

The basic idea of this review is to study the bottomonia production in p-p and A-A collisions.

[Will write this after section 2 is complete]

In section 3 we have reviewed the bottomonia production mechanism in p-p collisions. The bottomonia or in general quarkonia production in p-p or A-A collisions consists of two sub processes. First, the heavy quark pairs are produced through a perturbative process and then these heavy quarks form quarkonia through a non-perturbative process. We have discussed the basic aspects of the perturbative production of heavy quarks. Since the formation of bottomonia is a non-perturbative process one has to take recourse to some effective models. We have discussed the color singlet model, the color evaporation model and the NRQCD factorisation approach. In color singlet model it is assumed that the $Q\bar{Q}$ pair that evolves into the quarkonium is in a color-singlet state. It is further assumed that $Q\bar{Q}$ pair has the same spin and angular-momentum quantum numbers as the quarkonium. On the other hand in the color evaporation model it is assumed that every produced $Q\overline{Q}$ pair evolves into a quarkonium if it has an invariant mass that is less than the threshold for producing a pair of open-flavor heavy mesons. The CEM prediction is found to be in good agreement with the CDF data. We have studied NRQCD formalism in quite amount of detail. The NRQCD formalism, along with color singlet state, includes the colour octet state. In this formalism the evolution probability of $Q\bar{Q}$ pair into a state of quarkonium is expressed as matrix elements of NRQCD operators expanded in terms of heavy quark velocity v. We have discussed the Υ(ns) production $p + p$ collision at $\sqrt{s} = 13$ TeV and at $\sqrt{s} = 7$ TeV. The feeddown contributions have been accounted for.

In section 4 we have presented an experimental overview of the bottomonia results at RHIC and LHC. We have looked into the R_{AA} for Υ(ns) as a functions of p_T, y and N_{part}. We have also studied v_2 for these states with centrality and p_T.

In section 5 we have discussed the production of bottomonia in heavy ion collisions. We have started the first

proposal of Matsui and Satz for the suppression of quarkonia in the medium. Then we have discussed the more recent ideas like sequential suppression. The cold nuclear matter has been reviewed in certain amount of detail. In section 5.3 we have discussed the kinetic approach. We have presented the theoretical results of R_{AA} and compared those with the experimentally available data from CMS and ALICE. In section 5.4 we have discussed the transport approach in the bottomonia production. One again the results have been compared with the CMS data. Section 5.5 deals with the suppression in the anisotropic medium. The results of R_{AA} in the anisotropic medium have been presented and compared with the CMS data.

References

[1] E. V. Shuryak, Quantum Chromodynamics and the Theory of Superdense Matter, Phys. Rept. 61 (1980) 71–158. doi:10.1016/0370-1573(80)90105-2.

[2] H. Satz, The Quark-Gluon Plasma: A Short Introduction, Nucl. Phys. A 862-863 (2011) 4–12. arXiv:1101.3937, doi:10.1016/j.nuclphysa.2011.05.014.

[3] H. Satz, Color deconfinement in nuclear collisions, Rept. Prog. Phys. 63 (2000) 1511. arXiv:hep-ph/0007069, doi:10.1088/0034-4885/63/9/203.

[4] T. Matsui, H. Satz, J/ψ Suppression by Quark-Gluon Plasma Formation, Phys. Lett. B 178 (1986) 416–422. doi:10.1016/0370-2693(86)91404-8.

[5] L. Kluberg, 20 years of J/psi suppression at the CERN SPS: Results from experiments NA38, NA51 and NA50, Eur. Phys. J. C 43 (2005) 145–156. doi:10.1140/epjc/s2005-02245-6.

[6] A. M. Sirunyan, et al., Measurement of prompt and nonprompt charmonium suppression in PbPb collisions at 5.02 TeV, Eur. Phys. J. C 78 (6) (2018) 509. arXiv:1712.08959, doi:10.1140/epjc/s10052-018-5950-6.

[7] A. M. Sirunyan, et al., Suppression of Excited Υ States Relative to the Ground State in Pb-Pb Collisions at $\sqrt{s_{\mathrm{NN}}}$=5.02 TeV, Phys. Rev. Lett. 120 (14) (2018) 142301. arXiv:1706.05984, doi:10.1103/PhysRevLett.120.142301.

[8] A. M. Sirunyan, et al., Measurement of nuclear modification factors of Υ(1S), Υ(2S), and Υ(3S) mesons in PbPb collisions at $\sqrt{s_{\mathrm{NN}}} = 5.02$ TeV, Phys. Lett. B 790 (2019) 270–293. arXiv:1805.09215, doi:10.1016/j.physletb.2019.01.006.

[9] S. Acharya, et al., Studies of J/ψ production at forward rapidity in Pb-Pb collisions at $\sqrt{s_{\mathrm{NN}}} = 5.02$ TeV, JHEP 02 (2020) 041. arXiv:1909.03158, doi:10.1007/JHEP02(2020)041.

[10] S. Acharya, et al., Υ suppression at forward rapidity in Pb-Pb collisions at $\sqrt{s_{\mathrm{NN}}} = 5.02$ TeV, Phys. Lett. B 790 (2019) 89–101. arXiv:1805.04387, doi:10.1016/j.physletb.2018.11.067.

[11] M. Strickland, Thermal υ_{1s} and chi_b1 suppression in $\sqrt{s_{NN}} = 2.76$ TeV Pb-Pb collisions at the LHC, Phys. Rev. Lett. 107 (2011) 132301. arXiv:1106.2571, doi:10.1103/PhysRevLett.107.132301.

[12] T. Song, K. C. Han, C. M. Ko, Bottomonia suppression in heavy-ion collisions, Phys. Rev. C 85 (2012) 014902. arXiv:1109.6691, doi:10.1103/PhysRevC.85.014902.

[13] V. Kumar, P. Shukla, R. Vogt, Quarkonia suppression in PbPb collisions at $\sqrt{s_{NN}}$ = 2.76 TeV, Phys. Rev. C 92 (2) (2015) 024908. arXiv:1410.3299, doi:10.1103/PhysRevC.92.024908.

[14] V. Kumar, P. Shukla, A. Bhattacharyya, Suppression of quarkonia in PbPb collisions at $\sqrt{s_{NN}} = 5.02$ TeV, J. Phys. G 47 (1) (2020) 015104. arXiv:1909.10785, doi:10.1088/1361-6471/ab51cf.

[15] S. Chatrchyan, et al., Indications of suppression of excited Υ states in PbPb collisions at $\sqrt{S_{NN}}$ = 2.76 TeV, Phys. Rev. Lett. 107 (2011) 052302. arXiv:1105.4894, doi:10.1103/PhysRevLett.107.052302.

[16] S. Chatrchyan, et al., Observation of Sequential Upsilon Suppression in PbPb Collisions, Phys. Rev. Lett. 109 (2012) 222301, [Erratum: Phys.Rev.Lett. 120, 199903 (2018)]. arXiv:1208.2826, doi:10.1103/PhysRevLett.109.222301.

[17] S. Acharya, et al., Υ suppression at forward rapidity in Pb-Pb collisions at $\sqrt{s_{NN}}$ = 5.02 TeV, Phys. Lett. B 790 (2019) 89–101. arXiv:1805.04387, doi:10.1016/j.physletb.2018.11.067.

[18] L. Adamczyk, et al., Suppression of Υ production in d+Au and Au+Au collisions at $\sqrt{s_{NN}}$=200 GeV, Phys. Lett. B 735 (2014) 127–137, [Erratum: Phys.Lett.B 743, 537–541 (2015)]. arXiv:1312.3675, doi:10.1016/j.physletb.2014.06.028.

[19] S. W. Herb, D. C. Hom, L. M. Lederman, J. C. Sens, H. D. Snyder, J. K. Yoh, J. A. Appel, B. C. Brown, C. N. Brown, W. R. Innes, K. Ueno, T. Yamanouchi, A. S. Ito, H. Jöstlein, D. M. Kaplan, R. D. Kephart, Observation of a dimuon resonance at 9.5 gev in 400-gev proton-nucleus collisions, Phys. Rev. Lett. 39 (1977) 252–255. doi:10.1103/PhysRevLett.39.252.
URL https://link.aps.org/doi/10.1103/PhysRevLett.39.252

[20] F. Abe, et al., Υ production in $p\bar{p}$ collisions at $\sqrt{s}$ = 1.8 TeV, Phys. Rev. Lett. 75 (1995) 4358. doi:10.1103/PhysRevLett.75.4358.

[21] D. Acosta, et al., Υ Production and Polarization in $p\bar{p}$ Collisions at $\sqrt{s}$ = 1.8-TeV, Phys. Rev. Lett. 88 (2002) 161802. doi:10.1103/PhysRevLett.88.161802.

[22] V. M. Abazov, et al., Measurement of inclusive differential cross sections for Υ_{1S} production in $p\bar{p}$ collisions at $\sqrt{s}$ = 1.96-TeV, Phys. Rev. Lett. 94 (2005) 232001, [Erratum: Phys.Rev.Lett. 100, 049902 (2008)]. arXiv:hep-ex/0502030, doi:10.1103/PhysRevLett.94.232001.

[23] V. Khachatryan, et al., Upsilon Production Cross-Section in pp Collisions at $\sqrt{s}$=7 TeV, Phys. Rev. D 83 (2011) 112004. arXiv:1012.5545, doi:10.1103/PhysRevD.83.112004.

[24] V. Khachatryan, et al., Measurements of the Υ(1S), Υ(2S), and Υ(3S) differential cross sections in pp collisions at $\sqrt{s}$ = 7 TeV, Phys. Lett. B 749 (2015) 14–34. arXiv:1501.07750, doi:10.1016/j.physletb.2015.07.037.

[25] G. Aad, et al., Measurement of Upsilon production in 7 TeV pp collisions at ATLAS, Phys. Rev. D 87 (5) (2013) 052004. arXiv:1211.7255, doi:10.1103/PhysRevD.87.052004.

[26] V. M. Abazov, et al., Measurement of the polarization of the $\Upsilon(1S)$ and $\Upsilon(2S)$ states in $p\bar{p}$ collisions at $\sqrt{s}$ = 1.96-TeV, Phys. Rev. Lett. 101 (2008) 182004. arXiv:0804.2799, doi:10.1103/PhysRevLett.101.182004.

[27] T. Aaltonen, et al., Measurements of Angular Distributions of Muons From Υ Meson Decays in $p\bar{p}$ Collisions at $\sqrt{s}$ = 1.96 TeV, Phys. Rev. Lett. 108 (2012) 151802. arXiv:1112.1591, doi:10.1103/PhysRevLett.108.151802.

[28] S. Chatrchyan, et al., Measurement of the $Y(1S)$, $Y(2S)$ and $Y(3S)$ Polarizations in pp Collisions at $\sqrt{s} = 7$ TeV, Phys. Rev. Lett. 110 (8) (2013) 081802. arXiv:1209.2922, doi:10.1103/PhysRevLett.110.081802.

[29] G. Aad, et al., Measurement of the $\Upsilon(1S)$ production cross-section in pp collisions at $\sqrt{s} = 7$ TeV in ATLAS, Phys. Lett. B 705 (2011) 9–27. arXiv:1106.5325, doi:10.1016/j.physletb.2011.09.092.

[30] S. Chatrchyan, et al., Measurement of the $\Upsilon(1S)$, $\Upsilon(2S)$, and $\Upsilon(3S)$ Cross Sections in pp Collisions at $\sqrt{s} = 7$ TeV, Phys. Lett. B 727 (2013) 101–125. arXiv:1303.5900, doi:10.1016/j.physletb.2013.10.033.

[31] A. M. Sirunyan, et al., Measurement of quarkonium production cross sections in pp collisions at $\sqrt{s} = 13$ TeV, Phys. Lett. B 780 (2018) 251–272. arXiv:1710.11002, doi:10.1016/j.physletb.2018.02.033.

[32] P. Nason, S. Dawson, R. K. Ellis, The One Particle Inclusive Differential Cross-Section for Heavy Quark Production in Hadronic Collisions, Nucl. Phys. B 327 (1989) 49–92, [Erratum: Nucl.Phys.B 335, 260–260 (1990)]. doi:10.1016/0550-3213(89)90286-1.

[33] G. T. Bodwin, E. Braaten, G. P. Lepage, Rigorous QCD analysis of inclusive annihilation and production of heavy quarkonium, Phys. Rev. D 51 (1995) 1125–1171, [Erratum: Phys.Rev.D 55, 5853 (1997)]. arXiv:hep-ph/9407339, doi:10.1103/PhysRevD.55.5853.

[34] N. Brambilla, et al., QCD and Strongly Coupled Gauge Theories: Challenges and Perspectives, Eur. Phys. J. C 74 (10) (2014) 2981. arXiv:1404.3723, doi:10.1140/epjc/s10052-014-2981-5.

[35] M. B. Einhorn, S. D. Ellis, Hadronic Production of the New Resonances: Probing Gluon Distributions, Phys. Rev. D 12 (1975) 2007. doi:10.1103/PhysRevD.12.2007.

[36] E. L. Berger, D. L. Jones, Inelastic Photoproduction of J/psi and Upsilon by Gluons, Phys. Rev. D 23 (1981) 1521–1530. doi:10.1103/PhysRevD.23.1521.

[37] H. Fritzsch, Producing Heavy Quark Flavors in Hadronic Collisions: A Test of Quantum Chromodynamics, Phys. Lett. B 67 (1977) 217–221. doi:10.1016/0370-2693(77)90108-3.

[38] J. F. Amundson, O. J. P. Eboli, E. M. Gregores, F. Halzen, Colorless states in perturbative QCD: Charmonium and rapidity gaps, Phys. Lett. B 372 (1996) 127–132. `arXiv:hep-ph/9512248`, `doi:10.1016/0370-2693(96)00035-4`.

[39] P. Nason, S. Dawson, R. K. Ellis, The Total Cross-Section for the Production of Heavy Quarks in Hadronic Collisions, Nucl. Phys. B 303 (1988) 607–633. `doi:10.1016/0550-3213(88)90422-1`.

[40] N. Brambilla, et al., Heavy quarkonium physics`arXiv:hep-ph/0412158`, `doi:10.5170/CERN-2005-005`.

[41] S. D. Ellis, M. B. Einhorn, C. Quigg, Comment on Hadronic Production of Psions, Phys. Rev. Lett. 36 (1976) 1263. `doi:10.1103/PhysRevLett.36.1263`.

[42] C. E. Carlson, R. Suaya, Hadronic Production of psi/J Mesons, Phys. Rev. D 14 (1976) 3115. `doi:10.1103/PhysRevD.14.3115`.

[43] G. A. Schuler, Quarkonium production and decays, Ph.D. thesis, Hamburg U. (1994). `arXiv:hep-ph/9403387`.

[44] P. Artoisenet, J. P. Lansberg, F. Maltoni, Hadroproduction of J/ψ and Υ in association with a heavy-quark pair, Phys. Lett. B 653 (2007) 60–66. `arXiv:hep-ph/0703129`, `doi:10.1016/j.physletb.2007.04.031`.

[45] J. M. Campbell, F. Maltoni, F. Tramontano, QCD corrections to J/psi and Upsilon production at hadron colliders, Phys. Rev. Lett. 98 (2007) 252002. `arXiv:hep-ph/0703113`, `doi:10.1103/PhysRevLett.98.252002`.

[46] P. Artoisenet, J. M. Campbell, J. P. Lansberg, F. Maltoni, F. Tramontano, Υ Production at Fermilab Tevatron and LHC Energies, Phys. Rev. Lett. 101 (2008) 152001. `arXiv:0806.3282`, `doi:10.1103/PhysRevLett.101.152001`.

[47] J. F. Amundson, O. J. P. Eboli, E. M. Gregores, F. Halzen, Quantitative tests of color evaporation: Charmonium production, Phys. Lett. B 390 (1997) 323–328. `arXiv:hep-ph/9605295`, `doi:10.1016/S0370-2693(96)01417-7`.

[48] H.-L. Lai, J. Guzzi, Marco an dHuston, Z. Li, P. M. Nadolsky, J. Pumplin, C. P. Yuan, New parton distributions for collider physics, Phys. Rev. D`arXiv:1007.2241`, `doi:10.1103/PhysRevD.82.074024`.

[49] R. E. Nelson, R. Vogt, A. D. Frawley, Narrowing the uncertainty on the total charm cross section and its effect on the J/ψ cross section, Phys. Rev. C 87 (1) (2013) 014908. `arXiv:1210.4610`, `doi:10.1103/PhysRevC.87.014908`.

[50] K. J. Eskola, H. Paukkunen, C. A. Salgado, EPS09: A New Generation of NLO and LO Nuclear Parton Distribution Functions, JHEP 04 (2009) 065. `arXiv:0902.4154`, `doi:10.1088/1126-6708/2009/04/065`.

[51] V. Kumar, P. Shukla, R. Vogt, Components of the dilepton continuum in Pb+Pb collisions at $\sqrt{s_{NN}} = 2.76$ TeV, Phys. Rev. C 86 (2012) 054907. `arXiv:1205.3860`, `doi:10.1103/PhysRevC.86.054907`.

[52] S. Chatrchyan, et al., Observation and studies of jet quenching in PbPb collisions at nucleon-nucleon center-of-mass energy = 2.76 TeV, Phys. Rev. C 84 (2011) 024906. `arXiv:1102.1957`, `doi:10.1103/PhysRevC.84.024906`.

[53] J. L. Domenech, M. A. Sanchis-Lozano, Bottomonium production at the Tevatron and the LHC, Phys. Lett. B 476 (2000) 65–72. `arXiv:hep-ph/9911332`, `doi:10.1016/S0370-2693(00)00119-2`.

[54] J. L. Domenech, M. A. Sanchis-Lozano, Results from bottomonia production at the Tevatron and prospects for the LHC, Nucl. Phys. B 601 (2001) 395–421. `arXiv:hep-ph/0012296`, `doi:10.1016/S0550-3213(01)00053-0`.

[55] E. Braaten, S. Fleming, A. K. Leibovich, NRQCD analysis of bottomonium production at the Tevatron, Phys. Rev. D 63 (2001) 094006. `arXiv:hep-ph/0008091`, `doi:10.1103/PhysRevD.63.094006`.

[56] B. Gong, J.-X. Wang, H.-F. Zhang, QCD corrections to Υ production via color-octet states at the Tevatron and LHC, Phys. Rev. D 83 (2011) 114021. `arXiv:1009.3839`, `doi:10.1103/PhysRevD.83.114021`.

[57] R. Sharma, I. Vitev, High transverse momentum quarkonium production and dissociation in heavy ion collisions, Phys. Rev. C 87 (4) (2013) 044905. `arXiv:1203.0329`, `doi:10.1103/PhysRevC.87.044905`.

[58] B. Gong, L.-P. Wan, J.-X. Wang, H.-F. Zhang, Complete next-to-leading-order study on the yield and polarization of $\Upsilon(1S, 2S, 3S)$ at the Tevatron and LHC, Phys. Rev. Lett. 112 (3) (2014) 032001. `arXiv:1305.0748`, `doi:10.1103/PhysRevLett.112.032001`.

[59] Y. Feng, B. Gong, L.-P. Wan, J.-X. Wang, An updated study of Υ production and polarization at the Tevatron and LHC, Chin. Phys. C 39 (12) (2015) 123102. `arXiv:1503.08439`, `doi:10.1088/1674-1137/39/12/123102`.

[60] H. Han, Y.-Q. Ma, C. Meng, H.-S. Shao, Y.-J. Zhang, K.-T. Chao, $\Upsilon(nS)$ and $\chi_b(nP)$ production at hadron colliders in nonrelativistic QCD, Phys. Rev. D 94 (1) (2016) 014028. `arXiv:1410.8537`, `doi:10.1103/PhysRevD.94.014028`.

[61] G.-M. Yu, Y.-B. Cai, Y.-D. Li, J.-S. Wang, Heavy quarkonium photoproduction in ultrarelativistic heavy ion collisions, Phys. Rev. C 95 (1) (2017) 014905, [Addendum: Phys.Rev.C 95, 069901 (2017)]. `arXiv:1703.03194`, `doi:10.1103/PhysRevC.95.014905`.

[62] D. Acosta, et al., Υ Production and Polarization in $p\bar{p}$ Collisions at $\sqrt{s} = 1.8$-TeV, Phys. Rev. Lett. 88 (2002) 161802. `doi:10.1103/PhysRevLett.88.161802`.

[63] R. Aaij, et al., Measurement of Upsilon production in pp collisions at $\sqrt{s} = 7$ TeV, Eur. Phys. J. C 72 (2012) 2025. `arXiv:1202.6579`, `doi:10.1140/epjc/s10052-012-2025-y`.

[64] V. Khachatryan, et al., Measurements of the $\Upsilon(1S)$, $\Upsilon(2S)$, and $\Upsilon(3S)$ differential cross sections in pp collisions at $\sqrt{s} = 7$ TeV, Phys. Lett. B 749 (2015) 14–34. arXiv:1501.07750, doi:10.1016/j.physletb.2015.07.037.

[65] G. Aad, et al., Measurement of Upsilon production in 7 TeV pp collisions at ATLAS, Phys. Rev. D 87 (5) (2013) 052004. arXiv:1211.7255, doi:10.1103/PhysRevD.87.052004.

[66] S. Chatrchyan, et al., Measurement of the $\Upsilon(1S)$, $\Upsilon(2S)$, and $\Upsilon(3S)$ Cross Sections in pp Collisions at $\sqrt{s} = 7$ TeV, Phys. Lett. B 727 (2013) 101–125. arXiv:1303.5900, doi:10.1016/j.physletb.2013.10.033.

[67] A. M. Sirunyan, et al., Measurement of quarkonium production cross sections in pp collisions at $\sqrt{s} = 13$ TeV, Phys. Lett. B 780 (2018) 251–272. arXiv:1710.11002, doi:10.1016/j.physletb.2018.02.033.

[68] V. Kumar, P. Shukla, Charmonia production in p + p collisions under NRQCD formalism, J. Phys. G 44 (8) (2017) 085003. arXiv:1606.08265, doi:10.1088/1361-6471/aa7818.

[69] R. Baier, R. Ruckl, Hadronic Collisions: A Quarkonium Factory, Z. Phys. C 19 (1983) 251. doi:10.1007/BF01572254.

[70] B. Humpert, NARROW HEAVY RESONANCE PRODUCTION BY GLUONS, Phys. Lett. B 184 (1987) 105–107. doi:10.1016/0370-2693(87)90496-5.

[71] R. Gastmans, W. Troost, T. T. Wu, Production of Heavy Quarkonia From Gluons, Nucl. Phys. B 291 (1987) 731. doi:10.1016/0550-3213(87)90493-7.

[72] P. L. Cho, A. K. Leibovich, Color octet quarkonia production, Phys. Rev. D 53 (1996) 150–162. arXiv:hep-ph/9505329, doi:10.1103/PhysRevD.53.150.

[73] P. L. Cho, A. K. Leibovich, Color octet quarkonia production. 2., Phys. Rev. D 53 (1996) 6203–6217. arXiv:hep-ph/9511315, doi:10.1103/PhysRevD.53.6203.

[74] T.-J. Hou, et al., New CTEQ global analysis of quantum chromodynamics with high-precision data from the LHC, Phys. Rev. D 103 (1) (2021) 014013. arXiv:1912.10053, doi:10.1103/PhysRevD.103.014013.

[75] B. B. Abelev, et al., Suppression of $\Upsilon(1S)$ at forward rapidity in Pb-Pb collisions at $\sqrt{s_{NN}} = 2.76$ TeV, Phys. Lett. B 738 (2014) 361–372. arXiv:1405.4493, doi:10.1016/j.physletb.2014.10.001.

[76] V. Khachatryan, et al., Suppression of $\Upsilon(1S)$, $\Upsilon(2S)$ and $\Upsilon(3S)$ production in PbPb collisions at $\sqrt{s_{NN}} = 2.76$ TeV, Phys. Lett. B 770 (2017) 357–379. arXiv:1611.01510, doi:10.1016/j.physletb.2017.04.031.

[77] A. M. Sirunyan, et al., Measurement of nuclear modification factors of $\Upsilon(1S)$, $\Upsilon(2S)$, and $\Upsilon(3S)$ mesons in PbPb collisions at $\sqrt{s_{\mathrm{NN}}} = 5.02$ TeV, Phys. Lett. B 790 (2019) 270–293. `arXiv:1805.09215`, `doi:10.1016/j.physletb.2019.01.006`.

[78] S. Acharya, et al., Υ production and nuclear modification at forward rapidity in Pb-Pb collisions at $\sqrt{s_{\mathrm{NN}}} = 5.02$ TeV, Phys. Lett. B 822 (2021) 136579. `arXiv:2011.05758`, `doi:10.1016/j.physletb.2021.136579`.

[79] P. Wang, Υ measurements in Au+Au collisions at $\sqrt{s_{NN}} = 200$GeV with the STAR experiment, Nucl. Phys. A 982 (2019) 723–726. `doi:10.1016/j.nuclphysa.2018.09.025`.

[80] L. He, T. Edmonds, Z.-W. Lin, F. Liu, D. Molnar, F. Wang, Anisotropic parton escape is the dominant source of azimuthal anisotropy in transport models, Phys. Lett. B 753 (2016) 506–510. `arXiv:1502.05572`, `doi:10.1016/j.physletb.2015.12.051`.

[81] S. Voloshin, Y. Zhang, Flow study in relativistic nuclear collisions by Fourier expansion of Azimuthal particle distributions, Z. Phys. C 70 (1996) 665–672. `arXiv:hep-ph/9407282`, `doi:10.1007/s002880050141`.

[82] A. M. Sirunyan, et al., Measurement of the azimuthal anisotropy of $\Upsilon(1S)$ and $\Upsilon(1S)$ mesons in PbPb collisions at $\sqrt{s_{\mathrm{NN}}} = 5.02$ TeV, Phys. Lett. B 819 (2021) 136385. `arXiv:2006.07707`, `doi:10.1016/j.physletb.2021.136385`.

[83] S. Acharya, et al., Measurement of $\Upsilon(1S)$ elliptic flow at forward rapidity in Pb-Pb collisions at $\sqrt{s_{\mathrm{NN}}} = 5.02$ TeV, Phys. Rev. Lett. 123 (19) (2019) 192301. `arXiv:1907.03169`, `doi:10.1103/PhysRevLett.123.192301`.

[84] S. Chatrchyan, et al., Event Activity Dependence of Y(nS) Production in $\sqrt{s_{NN}}$=5.02 TeV pPb and $\sqrt{s}$=2.76 TeV pp Collisions, JHEP 04 (2014) 103. `arXiv:1312.6300`, `doi:10.1007/JHEP04(2014)103`.

[85] A. Tumasyan, et al., Nuclear modification of Υ states in pPb collisions at $\sqrt{s_{\mathrm{NN}}} = 5.02$ TeV`arXiv:2202.11807`.

[86] A. M. Sirunyan, et al., Investigation into the event-activity dependence of $\Upsilon(nS)$ relative production in proton-proton collisions at $\sqrt{s} = 7$ TeV, JHEP 11 (2020) 001. `arXiv:2007.04277`, `doi:10.1007/JHEP11(2020)001`.

[87] S. Digal, P. Petreczky, H. Satz, Quarkonium feed-down and sequential suppression, Phys. Rev. D 64 (2001) 094015. `arXiv:0106017`.

[88] T. Umeda, K. Nomura, H. Matsufuru, Charmonium at finite temperature in quenched lattice QCD, Eur. Phys. J. C 39S1 (2005) 9. `arXiv:0211003`.

[89] M. Asakawa, T. Hatsuda, J/ψ and η_C in the deconfined plasma from lattice QCD `arXiv:0308034`.

[90] S. Datta, F. Karsch, P. Petreczky, I. Wetzorke, Behavior of charmonium systems after deconfinement , Phys. Rev. D 69 (2004) 094507. `arXiv:0312037`.

[91] A. Jakovác, P. Petreczky, K. Petrov, A. Velytsky, Quarkonium correlators and spectral functions at zero and finite temperature, Phys. Rev. D 75 (2007) 014506. `arXiv:0611017`.

[92] C. Allton, M. B. Oktay, M. Peardon, J. Skullerud, Charmonium at high temperature in two-flavor QCD, Phys. Rev. D 76 (2007) 094513. `arXiv:0705.2198`.

[93] C. Y. Wong, Heavy quarkonia in quark gluon plasma, Phys. Rev. C 72 (2005) 034906.

[94] A. Mócsy, P. Petreczky, Quarkonia correlators above deconfinement, Phys. Rev. D 73 (2006) 074007. `arXiv:0512156`.

[95] A. Mócsy, P. Petreczky, Heavy quarkonia survival in potential model, Eur. Phys. J. C 43 (2005) 77. `arXiv:0411262`.

[96] W. M. Alberico, A. Beraudo, A. D. Pace, A. Molinari, , Phys. Rev. D. 76 (2007) 114506.

[97] D. Cabrera, R. Rapp, T-matrix approach to quarkonium correlation functions in the QGP, Phys. Rev. D 76 (2007) 114506. `arXiv:0611134`.

[98] A. Mócsy, P. Petreczky, Can quarkonia survive deconfinement ? , Phys. Rev. D 77 (2008) 014501. `arXiv:0705.2559`.

[99] A. Mócsy, P. Petreczky, Color Screening Melts Quarkonium, Phys. Rev. Lett. 99 (2007) 211602. `arXiv:0705.2183`.

[100] M. Laine, O. Philipsen, M. Tassler, Thermal imaginary part of a real-time static potential from classical lattice gauge theory simulations, JHEP 0709 (2007) 066. `arXiv:0707.2458`.

[101] M. Laine, A resummed perturbative estimate for the quarkonium spectral function in hot QCD , JHEP 0705 (2007) 028. `arXiv:0704.1720`.

[102] M. Laine, How to compute the thermal quarkonium spectral function from first principles?, Nucl. Phys. A 820 (2009) 25C. `arXiv:0801.1112`.

[103] N. Brambilla, J. Ghiglieri, A. Vairo, P. Petreczky, Static quark-antiquark pairs at finite temperature, Phys. Rev. D 78 (2008) 014017. `arXiv:0804.0993`.

[104] P. Petreczky, Recent progress in lattice QCD at finite temperature`arXiv:0906.0502`.

[105] P. Petreczky, Quarkonium in Hot Medium, J. Phys. G. 37 (2010) 094009. `arXiv:1001.5284`.

[106] O. Kaczmarek, F. Karsch, P. Petreczky, F. Zantow, Heavy Quark Anti-Quark Free Energy and the Renormalized Polyakov Loop, Phys. Lett. B 543 (2002) 41. `arXiv:0207002`.

[107] C. Lourenco, R. Vogt, H. K. Woehri, Energy dependence of J/psi absorption in proton-nucleus collisions, JHEP 02 (2009) 014. `arXiv:0901.3054`, `doi:10.1088/1126-6708/2009/02/014`.

[108] R. L. Thews, M. Schroedter, J. Rafelski, Enhanced J/ψ production in deconfined quark matter, Phys. Rev. C 63 (2001) 054905. `arXiv:hep-ph/0007323`, `doi:10.1103/PhysRevC.63.054905`.

[109] G. Bhanot, M. E. Peskin, Short Distance Analysis for Heavy Quark Systems. 2. Applications, Nucl. Phys. B 156 (1979) 391–416. `doi:10.1016/0550-3213(79)90200-1`.

[110] F. Karsch, M. T. Mehr, H. Satz, Color Screening and Deconfinement for Bound States of Heavy Quarks, Z. Phys. C 37 (1988) 617. `doi:10.1007/BF01549722`.

[111] F. Arleo, P. B. Gossiaux, T. Gousset, J. Aichelin, Heavy quarkonium hadron cross-section in QCD at leading twist, Phys. Rev. D 65 (2002) 014005. `arXiv:hep-ph/0102095`, `doi:10.1103/PhysRevD.65.014005`.

[112] R. L. Thews, M. L. Mangano, Momentum spectra of charmonium produced in a quark-gluon plasma, Phys. Rev. C 73 (2006) 014904. `arXiv:nucl-th/0505055`, `doi:10.1103/PhysRevC.73.014904`.

[113] T. Affolder, et al., Production of $\Upsilon(1S)$ mesons from χ_b decays in $p\bar{p}$ collisions at $\sqrt{s} = 1.8$ TeV, Phys. Rev. Lett. 84 (2000) 2094–2099. `arXiv:hep-ex/9910025`, `doi:10.1103/PhysRevLett.84.2094`.

[114] M. Strickland, D. Bazow, Thermal Bottomonium Suppression at RHIC and LHC, Nucl. Phys. A 879 (2012) 25–58. `arXiv:1112.2761`, `doi:10.1016/j.nuclphysa.2012.02.003`.

[115] R. Vogt, M. Prakash, P. Koch, T. H. Hansson, J/ψ Interactions With Hot Hadronic Matter, Phys. Lett. B 207 (1988) 263–268. `doi:10.1016/0370-2693(88)90572-2`.

[116] M. Gluck, E. Reya, A. Vogt, Pionic parton distributions, Z. Phys. C 53 (1992) 651–656. `doi:10.1007/BF01559743`.

[117] L. Grandchamp, S. Lumpkins, D. Sun, H. van Hees, R. Rapp, , Physical. Rev. C (2006) 0649006.

[118] R. Rapp, X. Du, Theoretical Perspective on Quarkonia from SPS via RHIC to LHC, Nucl. Phys. A 967 (2017) 216–224. `arXiv:1704.07923`, `doi:10.1016/j.nuclphysa.2017.05.097`.

[119] L. Grandchamp, R. Rapp, , Nucl. Phys. A 709 (2002) 415.

[120] C. Flores, , Talk at Quark matter 2017.

[121] Y. Z. *et.al.*, , Nucl. Phys. A 967 (2017) 600.

[122] B. Krouppa, M. Strickland, Predictions for bottomonia suppression in 5.023 TeV Pb-Pb collisions, Universe 2 (3) (2016) 16. `arXiv:1605.03561`, `doi:10.3390/universe2030016`.

[123] B. Krouppa, A. Rothkopf, M. Strickland, Bottomonium suppression at RHIC and LHC, Nucl. Phys. A 982 (2019) 727–730. `arXiv:1807.07452`, `doi:10.1016/j.nuclphysa.2018.09.034`.

[124] A. Dumitru, Y. Guo, M. Strickland, , Phys. Lett. B 662 (2009) 37.

[125] O. Kaczmarek, F. Karsch, F. Zantow, P. Petreczky, , Phys. Rev. D 70 (2004) 074505.

[126] G. S. Bali, K. Schilling, A. Wachter, , Physical. Rev. D 56 (1997) 2566.